

Characteristics of an African Easterly Wave Observed During NAMMA

Robert Cifelli¹, Timothy Lang¹, Steven A. Rutledge¹, Nick Guy¹, Edward J. Zipser², Jon
Zawislak², and Robert Holzworth³

¹ *Department of Atmospheric Science, Colorado State University, Fort Collins, CO*

² *Department of Meteorology, University of Utah, Salt Lake, UT*

³ *Department of Atmospheric Science, University of Washington, Seattle, WA*

Corresponding Author Address:

Robert Cifelli

Department of Atmospheric Science

Colorado State University

Fort Collins, CO 80523-1371

970-491-8516 (V)

970-491-8449 (F)

rob@atmos.colostate.edu

Submitted to:

Journal of Atmospheric Science

TCSP-NAMMA Special Issue

ABSTRACT

The evolution of an African Easterly Wave is described using ground-based radar and ancillary data sets from 3 locations in West Africa: Niamey, Niger (continental), Dakar, Senegal (coastal), and Praia, Republic of Cape Verde (oceanic). The data were collected during the combined African Monsoon Multidisciplinary Analyses (AMMA) and NASA-AMMA (NAMMA) campaigns in August-September, 2006.

Two precipitation events originated within the wave circulation and propagated with the wave across west Africa. Mesoscale Convective Systems (MCSs) associated with these events were identified at all three sites ahead, within, and behind the 700 mb wave trough. An additional propagating event was identified that originated east of the wave and moved through the wave circulation. The MCS activity associated with this event did not show any appreciable change resulting from its interaction with the wave. The MCS characteristics at each site were different, likely due to a combination of life cycle effects and changes in relative phasing between the propagating systems and the position of low-level convergence and thermodynamic instability associated with the wave. At the ocean and coastal sites, the most intense convection occurred ahead of the wave trough where both high CAPE and low-level convergence were concentrated. At the continental site, convection was relatively weak due to fact that the wave dynamics and thermodynamics were not in synch when the systems passed through Niamey. The only apparent effect of the wave on MCS activity at the continental site was to extend the period of precipitation activity during one of the events that passed through coincident with the 700 mb wave trough. Convective organization at the land sites was primarily in the form of

squall line and linear MCSs oriented perpendicular to the low-level shear. The organization at the oceanic site was more complicated, transitioning from linear MCSs to widespread stratiform with embedded convection. The precipitation activity was also much longer lived at the oceanic site, due to the wave becoming nearly stationary near the Cape Verdes and providing an environment supportive of deep convection for an extended period.

1. Introduction

A significant fraction of rainfall in the Sahel region of west Africa occurs during the west African monsoon season (July-September). A substantial portion is associated with Mesoscale Convective Systems (MCSs). Indeed, Mathon et al. (2002) have shown that over 90% of the annual rainfall in parts of the central Sahel are associated with organized convection during Boreal summer.

Over west Africa and the eastern Atlantic, African Easterly Waves (AEWs) occur on a time scale of 3-6 days and are a fundamental component of west African climate (e.g., Burpee 1972, 1974; Reed et al. 1977; Thompson et al. 1979, and others). These westward moving disturbances modulate MCS activity and are therefore an important regulator of sub-seasonal rainfall variability in west Africa (e.g., Carlson, 1969a,b; Duvel 1990; Diedhiou et al. 1999; Mathon et al. 2002; Gu et al. 2004; Mekonnen et al. 2006; Futyán and Del Genio 2007). Using a combination of ECMWF and satellite data, Fink and Reiner (2003) found that over 40% of MCS squall lines in west Africa were forced by AEWs.

AEWs can often serve as the precursors to the formation of tropical cyclones in the eastern north Atlantic (e.g., Carlson, 1969a; Avila and Pasch, 1992; Thorncroft and Hodges 2001; Ross and Krishnamurti 2007; McTaggart. Et al. 2008). In particular Landsea (1993) and Chen et al. (2008) have shown that over 50% of the tropical cyclones in this region develop from AEWs, though the mechanism(s) that favor hurricane genesis from a particular AEW are not entirely

clear. Moreover, recent work has shown the importance of capturing transient AEWs in coupled climate models to obtain realistic precipitation variability in the Atlantic ITCZ (Seo et al. 2008).

Many of the above studies have examined the phasing between summertime precipitation in west Africa and AEW trough axes, showing that the phasing depends on the region of interest (e.g., Burpee 1974; Reed et al. 1977; Duvel 1990; Gu et al. 2004; Mathon et al. 2002; Fink and Reiner 2003). At latitudes south of 10-15° N, the location of convection shifts from northerly flow ahead of the trough (east of the Greenwich meridian) to southerly flow behind the trough in the eastern Atlantic. North of this latitude zone, precipitation primarily occurs in southerly flow behind the trough throughout the lifecycle of the AEW (Kiladis et al. 2006). More recent studies have examined the intensity and character of convection over continental west Africa and the maritime Atlantic, noting that the maritime systems tend to be weaker and more stratiform in nature compared to systems over the continent (Schumacher and Houze 2006; Futyan and Gel Genio 2007; Fuentes et al. 2008). Finally, Kiladis et al. (2006) have noted that diabatic processes are important to the energetics of AEWs north of 10-15°N and that these processes become less important south of this latitude belt.

Because observational platforms in west Africa are sparse, the above studies have generally relied on various combinations of models and satellite brightness temperature (OLR) data. More recently, the Tropical Rainfall Measuring Mission (TRMM) precipitation radar (PR) data have been used to examine AEW and precipitation characteristics over seasonal time scales and large geographic regions. Specific case studies of AEWs have been rare, especially at the mesoscale. However, case study analyses are sorely needed to better understand the feedback between

convection and AEWs as well as the role of AEWs in determining the interannual variability of precipitation during the West African Monsoon (Thorncroft and Hodges 2001; Berry and Thorncroft 2005).

During the summer of 2006, a large number of resources were deployed in west Africa and the eastern Atlantic to better understand the west African monsoon and its interactions across a variety of temporal and spatial scales. The 2006 field program over continental west Africa was part of the African Monsoon Multidisciplinary Analysis (AMMA – Redelsperger et al. 2006). Further “downstream” in the Cape Verde region off the coast of west Africa, the NASA-AMMA program (NAMMA – Zipser et al. 2009) was implemented in August-September 2006 to examine the interaction between AEWs, the Saharan Air Layer (SAL) and their role in tropical cyclogenesis. One of the important questions to be addressed by AMMA-NAMMA is the interaction of AEWs and convection associated with MCSs.

In this study, we examine the relationship of convection to an AEW as it moved over west Africa, crossed the coastline, and entered the oceanic environment. In particular, we make use of ground-based radar data from three locations (Niamey, Niger; Dakar, Senegal; and Praia, Cape Verde) during the AMMA-NAMMA campaign, representing three distinct geographical locations: continental, coastal, and maritime to explore the relationship between the wave and MCS precipitation characteristics in these geographically distinct environments. Our goal is to better understand how the horizontal and vertical structure of precipitation changes with geographical location. Because the vertical structure of precipitation is closely tied to diabatic heating which, in turn, feeds back to the evolution of the AEW, such information is critical for

understanding the role of MCS latent heating in the genesis, growth, and transition of some AEWs into tropical cyclones (Berry and Thorncroft 2006; Thorncroft et al. 2008). Observations of these processes are central to the objectives of NAMMA (Zipser et al. 2009).

All three radar sites are located between 13-15° N latitude (see Fig. 1), which for the continental and coastal sites, lies in the Sahel region where AEWs have a pronounced impact on squall line MCS generation (Fink and Reiner 2003). A recent study by Rickenbach et al. (2009) noted that more than half of the squall line MCSs observed by the radar in Niamey, Niger during AMMA were associated with AEW passages. Thus, the position of the radar sites provides an opportunity to analyze the phasing relationship between AEWs and precipitation in this transition latitudinal band.

2. Data and Methodology

During the NAMMA program, a total of 7 AEWs were identified (Zipser et al. 2009). For this study, AEW 5 (hereafter referred to as Wave 5) was chosen for detailed analysis for the simple reason that the wave was well sampled by sounding and radar data at all three locations.

European Centre for Medium-Range Forecasts (ECMWF) operational analyses (0.5 deg resolution, 4 times daily¹) were used to define the spatial extent of Wave 5 and to determine the timing of the ridge and trough at each radar location. To define the extent of Wave 5, the ECMWF 700 mb meridional wind was examined for the time period of interest (30 August – 4

¹ Available from the AMMA data user web site: <http://database.amma-international.org/>

September 2006) across west Africa and the eastern Atlantic (20°E to 40°W, 10°N to 20°N). Studies of AEWs have adopted many different techniques to define AEWs. Herein, we use the following simple criteria for identifying the wave. The extent of Wave 5 was defined as the location of the ridge (transition from southerly to northerly flow) ahead (west) of the trough (transition from northerly to southerly flow) to the ridge rearward (east) of the trough at 700 mb, based on ECMWF analyses. The mean latitude of all three radar sites (14°N) was used to determine the time of passage of different phases of Wave 5 at each site. Using this criteria, the total time period of influence of Wave 5 (ridge to ridge) varied from 72 hours at Niamey and Praia to 60 hours at Dakar (Table 1). Once the time period of Wave 5 was determined at each site with ECMWF analyses, the corresponding radar and sounding data were analyzed to examine precipitation characteristics and their relation to the environment (thermodynamics and shear) as a function of wave phase: ahead of the trough, within the trough passage, and to the rear of the trough.

Sounding data (up to 4 times daily during the lifecycle of Wave 5) was collected at all three sites corresponding to the radar locations (Praia [TOGA radar], Dakar [NPOL radar], and Niamey [MIT radar]). These data were quality controlled by the principal AMMA-NAMMA investigators for each sounding system. Examination of upper air sounding data at each location was used to cross-check the timing of Wave 5 based on operational analysis and showed good agreement to the trough passages (within 6 hours) determined with ECMWF data.

Radar data was obtained from two C-band systems (TOGA and MIT) and one S-band (NPOL). The MIT and TOGA systems are single polarimetric systems while NPOL has dual polarimetric

capability. However, only radar reflectivity was used for this study from the latter platform. All three radars operated nearly continuously during the August-September time period and performed similar scan sequences. MIT and TOGA scanned on a 10 minute repeat cycle and NPOL on a 15 minute repeat cycle, each collecting one multiple tilt volume scan during the repeat cycle (Table 2).

For all three radar systems, extensive quality control (QC) was performed to remove spurious echos (from ground and sea clutter) prior to analysis. Calibration of the radar reflectivity was accomplished via periodic internal calibrations and comparisons with the precipitation radar (PR) onboard the TRMM satellite during overpasses of the ground radar sites, following the procedure outlined in Lang et al. (2009). This comparison procedure is similar to the methodology described in Anagnostou et al. (2001). For TOGA, a 3.6 dB bias (high) with respect to the PR was found and was removed from the data set. The NPOL radar reflectivity was biased low relative to the PR and adjusted by 2 dB. For MIT, comparisons with the TRMM PR showed that the radar reflectivities were mostly within 1 dB of the PR and no correction was applied. Attenuation corrections were also applied to the C-band reflectivity data to account for signal loss in heavy rainfall. The attenuation algorithm of Patterson et al. (1979) was used. No attenuation correction was applied to the NPOL (S-band) system.

The radar data were then interpolated to a Cartesian grid using the NCAR REORDER software (Mohr et al., 1986) extending 120 km in x and y from a fixed point (13.5° N, 2.2° E for MIT, 14.7° N, 17.1° W for NPOL and 14.9° N, 23.5° W for TOGA) in the horizontal direction at 2 km vertical and horizontal resolution. The choice of grid resolution and maximum range were made

to reflect the fact that all three radars have different sampling characteristics (Table 2). In order to objectively compare radar echo features from the three data sets with different spatial resolution, the data were interpolated to a Cartesian grid such that the gridded resolution did not exceed the actual spatial resolution of any data set at maximum range. Thus, the maximum range was set as a compromise between obtaining as many echoes as possible and a resolution that allowed for reasonable identification of vertical and horizontal structure.

Precipitation features were identified in the radar data using an objective algorithm as described in Cifelli et al. (2007). Briefly, precipitation features were defined as contiguous regions of echo at the lowest grid level (1.5 km AGL) with radar reflectivity greater than or equal to 10 dBZ and containing at least 4 grid points. The 10 dBZ cutoff and minimum number of grid elements helped ensure that spurious echos missed during the QC procedure would not contaminate the analysis. The precipitation feature algorithm identified MCSs ($\geq 1000 \text{ km}^2$ and at least one convective grid point²), sub-MCSs ($< 1000 \text{ km}^2$ and at least one convective grid point), and NC (features that did not meet the convective element criteria regardless of their size). For each identified feature, statistics of rainfall rate at 1.5 km altitude, number of grid elements, and vertical structure (maximum height of selected radar reflectivity thresholds) were retained.

To estimate precipitation within each feature, power based radar reflectivity (Z) – rainfall relations of the form:

² Convective precipitation is defined using a reflectivity texture algorithm (Steiner et al. 1995). This algorithm uses both the echo intensity and the horizontal gradient of radar reflectivity to partition convective and stratiform precipitation.

$$Z = 230 * R^{1.25} \quad (TOGA) \quad (1)$$

$$Z = 368 * R^{1.24} \quad (NPOL) \quad (2)$$

$$Z = 364 * R^{1.36} \quad (MIT) \quad (3)$$

The TOGA Z-R is based on radar gauge comparisons for the GARP Atlantic Tropical Experiment (GATE) region (Hudlow 1978) and has been used for rainfall estimation in a number of tropical locations. The NPOL relation is taken from Nzeukou et al. (2004), based on disdrometer data in the Dakar region. The MIT relation comes from Niamey disdrometer data analyzed Sauvageot and Lacaux (1995). Use of different Z-R relations could introduce complications in the interpretation of results; however, the interest in this work is focused on trends as opposed to absolute differences. Moreover, sensitivity analyses showed that there is little change in the results when applying only one Z-R to all three radar data sets. The main difference is that the TOGA (GATE) relation produces more rain for a given reflectivity compared to the NPOL or MIT relations but this does not change the overall interpretation.

Data from the World Wide Lightning Location Network (WWLLN) are also used to indicate convective intensity during the passage of Wave 5 at each radar site. The WWLLN network uses a time of group arrival technique to analyze VLF (3-30 kHz) emissions from lightning flashes (Rodger et al. 2005). The Rodger et al. study found that the WWLLN detection efficiency for total lightning (intra-cloud and cloud-to-ground) over continental Africa to be about 3%. The location accuracy for this region is on the order of 3 km.

3. Results

A detailed overview of the 2006 African monsoon based on AMMA data analysis is provided in Janicot et al. (2008). For the purposes of this study we note that the 2006 season was characterized as being near normal in terms of rainfall and AEW activity. In particular, late August through September had slightly above average MCS activity across the Sahel region (11-17°N, 10°E-10°W) and was also the time period with the most coherent AEWs. The ITCZ was centered near 10°N.

a. Large-scale wave structure

Time-longitude diagrams of meridional wind and precipitation³ were used to compare the circulation and convective patterns of Wave 5 across west Africa and the east Atlantic. This wave was rather typical of similar disturbances observed during GATE in terms of speed and wavelength characteristics, though it must be remembered that most of the GATE studies represent composite wave structure – not individual wave characteristics (e.g., Reed et al. 1977). In terms of temperature deviations, Wave 5 was atypical of many of the GATE composite studies in that it had a cold core anomaly between 850 and 700 mb as it passed through Dakar and Praia (Zawislak and Zipser 2009). Zawislak and Zipser (2009) provide a comprehensive analysis of all the AEWs observed in NAMMA and the reader is referred to this study for a detailed description of all the NAMMA AEWs.

³ Precipitation is estimated from the TRMM satellite 3B42 product. TRMM 3B42 is a 3-hourly product produced through an optimal combination of SSM/I, TRMM TMI, AMSU, and AMSR satellite precipitation estimates. (see http://daac.gsfc.nasa.gov/precipitation/TRMM_README/TRMM_3B42_readme.shtml for more information).

The first appearance of a coherent circulation associated with Wave 5 was on 30 August (Fig. 2a) near 20°E. The wave traveled westward at approximately 8 m s⁻¹ with the 700 mb trough passing Niamey early on 31 August (Fig. 2 and Table 1). Across the continent, Wave 5 maintained a wavelength of 2,200-2,800 km. As the wave approached the west African coast on 2 September, there was an apparent “jump” in position, producing a kink in the meridional wind time series, making the position of the wave more difficult to track at this time (Fig. 2a). As the trough exited the coast and approached Praia on 3 September, the wave slowed down significantly and the circulation intensified. As shown in Fig. 2a, the wave remained nearly stationary for about 18 hours on 3 September in vicinity of the Cape Verdes before resuming its westward progression. Further tracking westward (not shown) indicated that Wave 5 may have interacted with a previous AEW disturbance (NAMMA Wave 4) near 55°W on 7 September. Although Hurricane Gordon initiated in this region on 10 September, it is not clear whether Wave 5 played a role in it’s formation (Zawislak and Zipser 2009).

The corresponding precipitation tracks associated with the wave are shown in Fig. 2b. These tracks represent propagating convective events as described by Laing et al. (2008). As discussed in the next section, two of the precipitation tracks traveled with Wave 5 (labeled “2” and “3”) and one event (labeled “1”) traveled faster, moving west of the wave circulation by the time it reached the continental site. Visible satellite data (not shown) indicate that each event was comprised of one or more MCSs embedded within a larger scale cloud shield, similar to the observations of Fortune (1980). All three tracks in Fig. 2b exhibited multiple oscillations in rainfall intensity, indicating that the MCSs passed through multiple periods of generation and decay as the events traversed across the continent. In general, rainfall maxima occurred in

proximity to high topography during the late afternoon-evening hours, in phase with the maximum of solar insolation. A relative minimum in rainfall activity was observed near the date line, possibly due to the lack of forcing by elevated terrain in this region (Laing et al. 2008). As discussed below, the relative position of the land radars with respect to the squall lines associated with the propagating events was an important factor in determining the MCS characteristics in these different geographic locations.

Throughout the lifecycle bracketing the three radar sites, Wave 5 maintained a complex dynamical structure. Between 31 August and 4 September, the AEW contained a primary vorticity center at 700 mb and one or more low-level vorticity centers (Fig. 1). Across the African continent, the low-level center(s) were often ahead (west) of the 700 mb trough. Moreover, the low-level vorticity centers straddled the AEJ (located near 15°N) and OLR data showed that the convection was associated primarily with the southern vortex. The complex vorticity evolution observed in Wave 5 is consistent with a number of previous studies examining AEW structure (Reed et al. 1988; Pytharoulis and Thorncroft 1999; Fink and Reiner 2003; Ross and Krishnamurti 2007). The low-level centers merged as Wave 5 moved into the eastern Atlantic on 3 September, coincident with an alignment of the low-level and 700 mb circulation centers and the reduction in wave speed described above. As discussed in Sec. 3d, this change in wave evolution allowed for the development of an extended period of precipitation activity at the oceanic site.

Finally, we note that the AEJ maintained a position relatively close to the latitude of the radar sites (near 15°N) across west Africa and east Atlantic from 31 August – 2 September but shifted

northward to near 20°N on 3 September. As discussed below in the following sections, the proximity of the AEJ had an important influence on the horizontal structure of precipitation (i.e., squall line vs non-squall line MCS) at the radar sites during the Wave 5 passage.

The next three sub-sections describe the precipitation and wave characteristics at each site in more detail.

b. Observations at the Continental Site (Niamey)

A time-height cross section of winds, relative humidity, and CAPE bracketing the passage of Wave 5 at Niamey is shown in Figure 3. The cross sections show that there was strong zonal shear associated with the proximity of the AEJ near 600 mb throughout the period but especially leading up to the trough passage (Fig. 3b). The meridional winds tilt westward with height from the surface to near 700 mb such that the near surface flow switches from southerly to northerly just ahead of the 700 mb trough passage (Fig. 3a). The northerly flow across the Sahel region reduced the moisture influx so that CAPE values remained low until after the arrival of the 700 mb trough (Fig. 3d).

The MIT radar observations identified three periods of precipitation activity during the passage of Wave 5 in Niamey. These events occurred in the early morning hours the day prior to the trough passage (Event 1), the day of the trough passage (Event 2), and the day after the trough passage (Event 3). The events can be seen in the precipitation Hövmöller diagram (Fig. 2b). Event 1 represents a propagating convective episode that initiated well east of the radar domains

(approximately 35°E near the Ethiopian highlands). As noted in Laing et al. (2008), propagating convective episodes often form in the lee of this high terrain region and are not necessarily associated with AEWs. This appears to be the case for the MCS activity associated with Event 1, which traveled westward at approximately 14 m s⁻¹ and eventually overtook Wave 5, moving into the leading (west) ridge by the time it reached Niamey on August 30. Similar observations of squall line MCSs that formed outside the region occupied by an AEW but later intercepted an AEW at some point during their lifecycle were reported by Fink and Reiner (2003). This emphasizes the difficulty in extracting the precipitation signal associated with an AEW.

The radar data indicated that the squall line associated with Event 1 contained a leading convective line and trailing stratiform region oriented perpendicular to the low-level shear vector (Fig. 4a). This is in agreement with LeMone et al. (1998) suggesting the importance of the lowest 200 mb in determining the orientation of the convective line. As it approached Niamey, the squall line rapidly weakened, probably as a result of dry conditions above the surface (Fig. 3c) as well as the decrease in intensity anticipated as the system propagated over night, away from the Joss plateau (Fig. 2b). The ECMWF analysis indicated that there was no appreciable large-scale lifting to support the convection as Event 1 passed through Niamey (Fig. 5a).

The precipitation Hövmöller shows that the Event 1 convective episode that was observed by MIT continued to move westward, ahead of Wave 5, and did not remain as part of the Wave 5 “envelope” (indicated by the labels “2” and “3”). In contrast to Fortune’s (1980) analysis, Event 1 did not undergo any obvious change as a result of its interaction with Wave 5. However, it likely did have an indirect impact on subsequent convection (Event 2) by modifying the local

moisture environment.

The Event 2 and 3 precipitation tracks are shown in Fig. 2b. Unlike Event 1, Events 2 and 3 propagated closer to the Wave 5 phase speed (10 m s^{-1}) and produced precipitation and brightness temperature (not shown) patterns that were similar to the Wave 5 meridional wind signature (Fig. 2a). It is therefore likely these propagating events represented precipitation events associated with Wave 5. Events 2 and 3 both initiated over the Joss plateau near 10°E in the Wave 5 trough zone and east of the trough, respectively. The Joss plateau is a highlands region that often spawns squall line MCSs during the summer months (Aspliden et al. 1976; Omotosho 1984; Rowell and Milford 1993; Fink and Reiner 2003; Rickenbach et al. 2009). Similar to Event 1, the overall MCS activity associated with Events 2 and 3 dissipated as the convection moved west of the Joss plateau and approached Niamey.

Event 2 was sampled at Niamey on 31 August coincident with the 700 mb wave trough passage. The upper air sounding data showed that, subsequent to the passage of Event 1 in Niamey, the mid-level environment near 700 mb moistened considerably but the CAPE was reduced (Fig. 3c,d). This was due to a combination of an influx of dry, northerly flow at low-levels and depletion of moisture from the passage of Event 1. The magnitude of the shear below 700 mb was $\sim 15 \text{ m s}^{-1}$, similar to conditions on the previous day (Fig. 3a,b). Similar to Event 1, Event 2 was characterized by a squall line MCS oriented perpendicular to the low-level shear vector. The intensity of this squall line was less than Event 1, with weaker echos along the leading edge of the convective line (Fig. 4b). The convective line decayed as the system arrived in Niamey, consistent with the less favorable environmental conditions present on 31 August. Although the

squall line collapsed, the radar data showed that weak precipitation lingered and that there was a resurgence of activity about 6 hours after the trough passage (Fig. 4c). The ECMWF analysis (Fig. 5d) indicated that a region of enhanced low-level convergence, located in the wave trough, was situated over the Niamey region at this time. The convergence and associated lifting may have aided in extending the overall period of precipitation activity on this day, despite the relatively unfavorable thermodynamic conditions.

Subsequent to the trough passage, there was a resurgence of moist southerly flow at low levels and the CAPE increased (Fig. 3a,d). As a consequence, Event 3 entered a more favorable environment for precipitation activity on 1 September compared to Event 2. The low-level shear was considerably reduced ($< 8 \text{ ms}^{-1}$) compared to the previous two days and the activity on this day was marked by a non-squall MCS (Fig. 4d) that was relatively short-lived. ECMWF analysis (not shown) indicated that there was little large-scale convergence to maintain convection in the vicinity of Niamey during the passage of Event 3 on 1 September.

Thus, at the continental site the convection associated with the passage of Wave 5 was relatively weak. This was apparently due to the fact that the necessary ingredients for deep, intense convection were not all present at the same time. Previous studies have demonstrated that the growth and intensity of many storms are dependent on factors such as shear, thermodynamic instability, and lifting (Weissman and Klemp 1986; Keenan and Carbone 1992; LeMone et al. 1998). In the case of the continental site, it appears that these factors, although present at different times, never occurred simultaneously. Moreover, both satellite and radar data indicate that the squall lines were all in their late (decay) stages of evolution by the time they crossed the

MIT radar domain.

c. Observations at the Coastal Site (Dakar)

Wave 5 continued to progress westward of Niamey, with the Event 2 and 3 MCS activity undergoing successive generation and decay in phase with the diurnal cycle (Fig. 2b). Visible satellite imagery showed that, around 14 UTC on 1 September, a squall line formed along the Guinea Highlands in conjunction with Event 2. This system went through a lifecycle very similar to the MCS described in Houze (1977) and Fortune (1980): an arc line with discrete convective elements formed west (ahead) of the main anvil cloud as the system developed. Over the next several hours, the arc line was ingested into the trailing cirrus shield and the whole system continued to intensify and advance westward. The main difference between the Event 2 squall line and the squall line analyzed by Fortune (1980) was the fact that the system studied herein travelled slower (about 10 m s^{-1}), closer to the overall speed of Wave 5, compared to the case studied by Fortune (1980), which traveled near 16 m s^{-1} and moved through an AEW.

About 7 hours prior to the 700 mb wave trough passage at Dakar (Fig. 6), the NPOL radar observed the squall line MCS (described above) associated with Event 2 entering the eastern part of the domain (Fig. 7a). At the time of the Event 2 arrival in the NPOL domain, the environment was primed for deep convection with moist southerly flow, large CAPE (Fig. 6), and enhanced low-level convergence over the region (Fig. 8a). Moreover, large shear below 700 mb (15 ms^{-1}) due to the proximity of the AEJ was conducive for organized MCS activity (Fig. 6b). Similar to the observations in Niamey, Event 2 was a squall line MCS oriented perpendicular to the low-

level shear vector.

The MCS was intense with reflectivity cores > 50 dBZ along the leading edge and a large region of trailing stratiform precipitation. The squall line also contained a significant rear inflow jet, with ground relative flow toward the radar (i.e, flow from east to west) exceeding 20 m s^{-1} down to ~ 0.8 km above the surface (Fig. 7b). The depth of rear inflow is similar to tropical squall line observations in west Africa collected during Convection Profonde Tropicale (COPT 81; Chong et al. 1986). Subsequent to the passage of the squall line, the Dakar sounding shows that the easterly flow below about 850 mb (~ 2.5 km AGL) increased, which was probably due to the strong rear inflow associated with the MCS.

The Event 2 squall line moved through the NPOL domain and continued westward, in proximity to the location of enhanced low-level convergence ahead of the wave trough (Fig. 8a). The WLLN data showed that the MCS maintained vigor for several hours as the squall line moved into the eastern Atlantic (Fig. 8b). After the squall line moved through, the environment dried out at low levels as the flow shifted to the north and the CAPE was significantly reduced by the time of the trough passage. Another period of MCS activity was observed starting about 7 hours after the trough passage, corresponding to Event 3 (Fig. 2b). As shown in Fig. 2b and discussed in Sec. 3e, the activity was weaker than the Event 2 squall line. The precipitation was organized as a linear MCS with a minimal trailing stratiform region (Fig. 7c). The lack of stratiform precipitation was probably due to the drier environment present above 700 mb at the time of the Event 3 passage.

d. Observations at the Oceanic Site (Praia)

As Wave 5 approached Praia, the phase speed was greatly reduced (Fig. 2) and a closed circulation pattern developed at both low (925 mb) and mid-levels (700 mb) south of the Cape Verdes. This development produced a gradual moistening of the lower and middle troposphere as the circulation centers moved into phase, allowing for an extended period of relatively high CAPE and instability (Fig. 9c,d). Coincident with the northward shift of the AEJ toward 20°N, low-level westerly flow developed ahead of the trough passage (Fig. 9b).

The TOGA radar observed the first signature of Event 2 late on 2 September as an area of enhanced low-level convergence ahead of the Wave 5 trough moved into the Praia region. The precipitation activity at this time had a complicated organization. In contrast to the land sites, lines of convection developed an orientation nearly parallel to the low-level shear (Fig. 10a). Although the entire complex of precipitation moved westward in the direction of Wave 5, cell motion at this time was from west to east, similar to the flow at 850 mb. Later on 3 September, the shear weakened considerably and the precipitation became less organized, being comprised of large areas of stratiform precipitation with embedded convection (Fig. 10b). According to the precipitation Hövmöller diagram (Fig. 2b), Event 3 arrived close to the time of the trough passage at Praia on 3 September. However as described below in Sec. 3e, the activity in the TOGA domain was continuous from the arrival of Event 2 for nearly 48 hours. The extended period of activity coincided with the merging of the north and south low-level vorticity centers (Fig. 11) as the wave trough lingered in the vicinity of the Cape Verdes and the circulation pattern intensified. The nearly stationary wave position around the Cape Verdes provided an

extended period of low-level convergence and associated rising motion over the TOGA domain.

e. Composite Analysis

The feature algorithm described in Sec. 2 was used to ascertain characteristics of the precipitation associated with the passage of Wave 5 at each site. As indicated in Table 3, MCSs contributed over 80% of the total rain volume at each location as well as the bulk of the total rain area. The fact that MCSs contributed the bulk of the rainfall during the passage of Wave 5 is in good agreement with space borne radar estimates (Nesbitt et al. 2006) and a number of studies from field campaigns in the east Atlantic (Houze and Cheng 1977; López 1978; Cheng and Houze 1979), east Pacific (Cifelli et al. 2007), and west Pacific (Rickenbach and Rutledge 1998).

However, with regard to the total contribution of convective precipitation, there are some differences between the results for Wave 5 and previous estimates in the west African region. In particular, the highest convective fractions were observed at the coastal and oceanic sites. This trend is opposite to space borne observations during the summer season, which indicate the largest convective fractions over the continent interior (Schumacher and Houze 2006). The lower convective fraction at the continental location is at least partly due to the contribution of the relatively weak precipitation associated with Events 2 and 3. Moreover, because of the small sample size used in this study, analysis of more AEWs are required to better understand the relationship between precipitation and wave evolution, a subject of future research.

To gain further insight into the precipitation characteristics at each site, time series of selected

parameters were constructed for each location during the Wave 5 period of influence. The time series were then normalized by the time of the trough passage so that the characteristics relative to the wave phase could be compared. The time series at each site encompass the leading ridge (ahead or west of trough) to the trailing ridge (rear or east of trough). It should be noted that, although the time series are shown for all features (MCS + sub-MCS), they are nearly equally applicable to MCS characteristics alone since MCSs were responsible for the bulk of the rainfall and precipitation area associated with Wave 5 (Table 3). This analysis builds on many previous case studies from GATE (Houze 1977; Zipser 1977; Gamache and Houze 1983; Leary 1984; Houze and Rappaport 1984; Wei and Houze 1987) that examined the relative contribution of convective and stratiform precipitation to overall MCS characteristics. Herein, we extend these GATE studies to explore the convective-stratiform contributions with respect to the phase of the AEW in more detail.

A comparison of total convective and stratiform precipitation areas is shown in Fig. 12. As expected, the stratiform peaks lag the convective peaks by several hours, reflecting the evolution of MCS features that passed through the radar domain at each site. Figure 12 also reveals the importance of stratiform echo to the total area of precipitation echo throughout the period of Wave 5 influence, consistent with the GATE studies cited above.

The relationship between echo area and wave phase is complicated. At the land sites, the relative position of MCS activity associated with Event 2 changes from within the 700 mb trough at Niamey to slightly ahead of the trough at Dakar. The position of Event 3 activity remains to the rear of the trough at both locations. The individual events are marked by a sharp build-up and

decay in echo coverage as precipitation moved through the radar domains primarily in the form of squall lines. These events were relatively short lived (< 8 hours). The exception to this trend was Event 2 at Niamey, coinciding with the 700 mb trough passage. The MCS activity in this event had the smallest peak convective echo coverage but persisted longer than the other Niamey events. As noted in Sec. 3b, the reduced coverage was likely due to the timing of the squall line passage with respect to the wave position.

At the ocean site, the precipitation activity was continuous starting with the arrival of Event 2. The convective area peaks about 7 hours ahead of the 700 mb trough passage and the stratiform area is a maximum during the wave passage. This phase relationship is similar to the pattern observed in Houze (1977) and Leary (1984) for a combined GATE squall line and cloud cluster event. The build-up of both convective and stratiform echo was noticeably more gradual compared to the land sites, reflecting the different character of precipitation at the oceanic site (linear bands transitioning to widespread stratiform echo with embedded convection). Moreover, the precipitation echo coverage at Praia extended for a much longer period (> 36 hours) than any of the events at either the continental or coastal sites. This build-up and decay period is similar to the evolution of the GATE events examined by Houze (1977) and Leary (1984). As noted in Sec. 3c, the slow build-up process and extended coverage period was due to a reduction in phase speed and change in structure as the wave exited the coast.

A comparison of the relative contribution of convective and stratiform rain volume with respect to the trough passage is shown in Fig. 13. The importance of convective precipitation to the overall rainfall total for the coastal and oceanic sites is clearly evident. Moreover, the bulk of the

rainfall occurred ahead of the 700 mb trough at these two locations, consistent with the timing of maximum low-level convergence (Figs. 8a and 11b). This is also the time of highest rain rates (not shown). The convective rain fractions for the coastal and oceanic sites (Table 3) are broadly consistent with similar statistics from a GATE squall line event (Wei and Houze 1987) that was evidently sampled in the vicinity of an AEW 700 mb trough (World Meteorological Organization, 1975).

The highest convective rain volume at the continental site also occurred ahead of the 700 mb trough in association with the Event 1 squall line passage. However, the Event 1 rain volume was about a factor of two lower than the convective rain volumes at the coastal and oceanic sites. The difference is likely due to the lower moisture in the mid-troposphere (Fig. 3c), leading to entrainment of dry air, as well as the lack of low-level convergence when Event 1 passed through the MIT radar domain. MCS activity associated with Events 2 and 3 at the continental site showed more of a balance between convective and stratiform precipitation compared to Event 1, in agreement with statistics from GATE squall lines sampled ahead of 700 mb AEW troughs (Houze 1977; Gamache and Houze 1983; Houze and Rappaport 1984).

Another metric of the convective intensity at each site is shown by the lightning flash rate time series (Fig. 14). The high flash rates ahead of the wave trough at the oceanic and coastal sites are consistent with the high convective rain volume fractions shown in Fig. 13. At these locations, the low-level convergence and favorable thermodynamic environment ahead of the wave trough were evidently conducive to the development of large updrafts and the presence of mixed phase precipitation as Event 2 propagated through the sampling domains. At the coastal

site, enhanced flash rates also occur in the southerly flow east of the trough in association with Event 3. At the continental site, lightning flash rates were relatively low in all of the convective episodes compared to the other sites. As noted above, this is likely a consequence of the timing of the event activity with respect to the wave location. At Niamey, none of the precipitation events benefited from the simultaneous effect of favorable thermodynamics and low-level convergence lifting.

In Fig. 15, we investigate the rain volume contribution of MCSs more closely, examining the relative contribution with mean maximum 20 dBZ⁴ echo top height. The plot shows that the contribution of rainfall is bimodal at all three radar sites: a peak near 7.5 km and a peak between 11-16 km. For the oceanic site, there is a nearly equal contribution of rainfall with relatively shallow (7.5 km) and deep (16 km) 20 dBZ echo top heights. Time series of echo top heights (not shown) indicated that the deep MCS rainfall contribution occurred ahead of the trough where the most favorable forcing (i.e., low-level convergence and CAPE) was concentrated. A similar trend was observed at the coastal site, though the rainfall contribution was more heavily skewed to deep MCSs. At the continental site, the rainfall vs. echo top trend is nearly opposite the coastal site with the majority of rainfall derived from relatively shallow MCSs. Previous studies using TRMM data (Geerts and Dejen3 2005; Schumacher and Houze 2006; Zipser et al. 2006; Fuentes et al. 2008)) have consistently shown that the Sahel region, including Niamey, has more vigorous convection compared to the eastern Atlantic. Thus, the MCS activity associated with Wave 5 during its passage across Niamey appears to have been atypical of the climatology for this region. The plot of sub-MCSs (Fig. 15b) shows the small rainfall contribution from these

⁴ 20 dBZ was chosen to minimize contamination from spurious echos that may have been missed in the radar QC.

features compared to MCSs. As expected, the sub-MCS rainfall is mostly derived from clouds with relatively shallow 20 dBZ echo top heights.

To investigate the vertical structure of precipitation in more detail, probability distributions (CFADs – Yuter and Houze 1995) of radar reflectivity were calculated from the radar data at each site during the passage of Wave 5 (Fig. 16). Throughout the vertical column, the intensity of convection is clearly largest at the coastal (NPOL) site, both in terms of the mean profile and the high-end portion of the distribution (Fig. 16b). Moreover, the gradient of reflectivity above the melting level is smallest at NPOL, suggesting an abundance of mixed phase precipitation associated with strong updrafts. This is consistent with the lightning frequency results shown in Fig. 14. An interesting difference between the oceanic vs. the land convective distributions is the increase in radar reflectivity toward the ground at the oceanic site. This suggests the importance of low-level drop growth and/or lack of evaporation at the ocean site compared to the land sites. The relatively uniform reflectivity profile at low-levels observed in the land sites suggests more of a balance of growth and break-up processes. Similar observations were reported by Fuentes et al. (2006) using TRMM data.

In the stratiform regions, the radar bright band signature is evident at both the continental and coastal locations but is weak at the ocean site. The greater intensity of the bright band at the land sites is likely due to the proximity of the AEJ and the resulting organized nature of convection that was observed over land (i.e., squall line MCSs) compared to the ocean. The bright band results primarily from the melting of aggregates as they descend through the 0°C level. Squall lines, with front-to-rear flow directed from the convective to stratiform region, would be

expected to transport ice particles rearward of the convective line at upper levels, which would then grow by vapor deposition in the presence of weak mesoscale ascent in the stratiform region (Rutledge and Houze 1987). Mesoscale lifting, forced by the convergence along the front-to-rear and rear inflow circulations, would promote the development of aggregates at lower levels in the mesoscale updraft. Upon melting, these particles would produce a sharp bright band signature.

Similar to the convective distributions, the stratiform reflectivity CFADs show a difference between the land and ocean sites at low-levels. A decrease of radar reflectivity toward the ground is clearly evident over the land sites, suggesting the importance evaporation and/or drop breakup in this region. This trend is not surprising, given the relatively high cloud bases over land compared to the ocean (Fuentes et al. 2006).

4. Conclusions

This study utilized data from a suite of observational platforms and operational analyses to examine the MCS characteristics associated with an AEW in three geographically distinct locations: continental (Niamey), coastal (Dakar), and oceanic (Praia). A unique aspect of the study was the incorporation of data from ground-based radars at each site to study the relationship between the wave and precipitation characteristics at widely separate locations and stages of the wave's lifetime.

Precipitation events ahead (west), within, and behind (east) the wave trough were identified in the radar data from all three sites. Satellite data showed that each event was comprised of one or

more squall line MCSs embedded within a larger scale cloud shield, similar to the observations from previous studies over west Africa. The intensity of the MCSs was modulated by the diurnal cycle and proximity to elevated terrain. The radar data showed that two of the events (identified as Events 2 and 3) were comprised of MCSs that originated over high terrain east of the continental site on successive days and propagated at roughly the phase speed within the circulation of the wave. At land sites, the AEJ was in close proximity and the events manifested primarily as squall line MCSs oriented perpendicular to the low-level shear. An additional propagating episode, Event 1, was also sampled at the continental site. This event originated over high terrain in east Africa and was apparently un-related to AEW activity. Event 1 propagated faster than the AEW, moving through Wave 5 and arriving in Niamey in the leading ridge of the wave. Other than the faster propagation speed, there were no apparent differences in the MCS characteristics associated with Event 1 compared to the MCSs that travelled with the AEW (associated with Events 2 and 3).

At the continental site, the MCSs were weak due to the fact that the systems arrived in the morning hours and were in their mature to decaying stages of evolution as they crossed the radar domain. None of the events benefited from the superposition of favorable thermodynamics and low-level convergence associated with the wave. The only apparent impact of the wave was to extend the period of activity of one of the squall lines (associated with Event 2). Although the convective line of this MCS collapsed as it moved through the MIT radar domain, weak precipitation lasted for an extended period (more than 12 hours). The extended period of activity appeared to be related to the proximity of the convergence lifting associated with the 700 mb wave trough passage coincident with the squall line activity.

At the coastal site, the MCS squall line associated with Event 2 arrived about 7 hours ahead of the 700 mb wave trough and entered an environment with moist, southerly flow and high CAPE. This was also a time when low-level convergence lifting was positioned near the Dakar region. Moreover, the proximity of the AEJ provided large zonal shear below 600 mb. Thus, the Event 2 squall line had a number of ingredients in place at the same time to support deep convection. Radar and satellite rainfall data also showed that the MCS was in an earlier, more intense phase of evolution as it crossed the coastal domain compared to the continental site. A squall line associated with Event 3 arrived about 6 hours after the passage of the 700 mb wave trough. This system was weaker than Event 2 due the fact that the environment was relatively dry (low CAPE) after the passage of the previous squall line and there was no apparent convergence forcing in the vicinity of Dakar at the time of Event 3's arrival.

As the wave exited the coast, it became nearly stationary and developed a closed circulation in close proximity to the oceanic site (Praia). This change in the wave structure provided an increasing influx of moisture over the Cape Verdes and pre-conditioned the environment for an extended period of precipitation activity (more than 36 hours). Although the signature of Events 2 and 3 were discernable from satellite data, from the TOGA radar perspective, the activity was continuous from the time Event 2 arrived at the oceanic site. Similar to the coastal site, the combined effects of large CAPE and lifting associated with the wave provided an environment conducive for deep convection ahead of the wave trough at the oceanic site. The main difference between the radar echo pattern at the ocean and land sites was that, at the ocean site, the shear became reduced as the AEJ shifted north and MCS activity switched from linear bands to

widespread stratiform with embedded convection.

An algorithm was used to objectively analyze radar precipitation features associated with the wave passage at each site. At all three locations, the precipitation characteristics were dominated by MCSs, which provided 69-78% of the area fraction and 84-89% of the rain volume fraction of precipitation. Further examination of the rain volume showed that over 70% was associated with convection at the coastal and oceanic sites but the fraction was closer to 50% at the continental site due to the relatively weak activity sampled during the wave passage. It was found that the rain volume at each location was derived from a combination of shallow and deep MCSs, though the proportion varied considerably (most shallow MCSs at the continental site and least at the coastal site). At the oceanic and coastal sites, the deepest MCSs generally occurred ahead of the trough in the high CAPE environment and were associated with the highest lightning frequency.

Comparisons of vertical structure in the convective and stratiform regions showed important differences at each site. In the convective region, the oceanic site had a signature of drop growth at low levels, which was not present at the other sites. In the stratiform region, the bright band was more intense at the land sites. It is hypothesized that this feature resulted from the advection of hydrometeors in the front-to-rear flow of the land-based squall lines. Moreover, an evaporation/drop break-up signature was identified at low levels in the land systems but did not occur in the oceanic system.

The results of this study are limited by the fact that only one AEW was examined. Future research should focus on examining additional precipitation events in different AEWs from the

NAMMA-AMMA program and compare the data more directly to previous satellite derived climatologies (e.g., TRMM). Moreover, it would be of interest to compare precipitation characteristics associated with waves that eventually become tropical cyclones against waves that do not become a named storm. Finally, the role of aerosols and dust and their role on convective intensity and longevity would be of interest to analyze.

Acknowledgments

The authors wish to thank Bob Houze, Chris Thorncroft and two anonymous reviewers for their valuable suggestions to improve the manuscript. This work was supported by the NASA Precipitation Measurement Mission under grant NNX06AC11G. The NAMMA program was made possible by Dr. Ramesh Kakar (NAMMA mission director). AMMA was built by an international scientific group and is currently funded by a large number of agencies, especially from France, UK, US and Africa. This study could not have been possible without the hard work and dedication of all AMMA-NAMMA participants. The ECMWF operational analysis and Niamey sounding data were made available from the AMMA science team via the AMMA data base web site. The sounding data at Niamey, Dakar, and Paria were provided by Doug Parker, Jose Fuentes, and the NASA Wallops Flight Facility, respectively. Steve Nesbitt provided the computer code to compare the ground radar data with corresponding TRMM overpass data and helped interpret the results for TOGA. Computer assistance from Paul Hein to derive a common format for all the sounding data was invaluable.

References

Anagnostou, E.N., C.A. Morales, and T. Dinku, 2001: The use of TRMM Precipitation Radar observations in determining ground radar calibration biases. *J. Atmos. Oceanic Technol.*, **18**, 616–628.

Aspliden C. I., Y. Tourre, and J. B. Sabine, 1976: Some climatological aspects of West African disturbance lines during GATE. *Mon. Wea. Rev.*, **104**, 1029–1035.

Avila L. A., and R. J. Pasch, 1992: Atlantic tropical systems of 1991. *Mon. Wea. Rev.*, **120**, 2688–2696.

Berry, G.J., and C. Thorncroft, 2005: Case study of an intense African easterly wave. *Mon. Wea. Rev.*, **133**, 752–766.

Burpee, R. W., 1972: The origin and structure of easterly waves in the lower troposphere of North Africa. *J. Atmos. Sci.*, **29**, 77-90.

Burpee, R. W., 1974: Characteristics of North African easterly waves during the summers of 1968 and 1969. *J. Atmos. Sci.*, **31**, 1556-1570.

Carlson T. N., 1969a: Synoptic histories of three African disturbances that developed into Atlantic hurricanes. *Mon. Wea. Rev.*, **97**, 256–275.

Carlson T. N., 1969b: Some remarks on African disturbances and their progress over tropical Atlantic. *Mon. Wea. Rev.*, **97**, 716–726.

Chen, T.-C., S.-Y. Wang, and A. J. Clark, 2008: North Atlantic hurricanes contributed by African Easterly Waves north and south of the African Easterly Jet. *J. Climate*, **21**, 6767-6776.

Cheng, C.P., and R.A. Houze, 1979: The distribution of convective and mesoscale precipitation in GATE radar echo patterns. *Mon. Wea. Rev.*, **107**, 1370–1381.

Chong M., P. Amayenc, G. Scialom, and J. Testud, 1987: A tropical squall line observed during the COPT 81 experiment in West Africa. Part I: Kinematic structure inferred from dual-Doppler radar data. *Mon. Wea. Rev.*, **115**, 670–694.

Cifelli, R., S.W. Nesbitt, S.A. Rutledge, W.A. Petersen, and S. Yuter, 2007: Radar characteristics of precipitation features in the EPIC and TEPPS regions of the east Pacific. *Mon. Wea. Rev.*, **135**, 1576-1595.

Diedhiou, A., S. Janicot, A. Viltard, P. de Felice, and H. Laurent, 1999: Easterly wave regimes and associated convection over West Africa and tropical Atlantic: Results from the NCEP/NCAR and ECMWF reanalyses., *Clim. Dyn.*, **15**, 795-822.

Duvel, J.P., 1990: Convection over Tropical Africa and the Atlantic Ocean during Northern Summer. Part II: Modulation by Easterly Waves. *Mon. Wea. Rev.* **118**, 1855–1868.

Ferreira, R. N., T. Rickenbach, N. Guy, and E. Williams, 2009: Radar observations of convective

system variability and interaction with African Easterly Waves during the 2006 AMMA IOP. *Mon. Wea. Rev.*, in review.

Fink, A. H., and A. Reiner (2003), Spatiotemporal variability of the relation between Africa easterly waves and West African squall lines in 1998 and 1999, *J. Geophys. Res.*, **108**(D11), 4332, DOI:10.1029/2002JD002816.

Fuentes, J. D., B. Geerts, T. Dejene, P. D.'Odorico, and E. Joseph, 2008: Vertical attributes of precipitation systems in West Africa and adjacent Atlantic Ocean. *Theor. Appl. Climatol.*, **92**, 181-193.

Futyan, J. M. and A. D. Del Genio, 2007: Deep convective system evolution over Africa and the tropical Atlantic. *J. Climate*, **20**, 5041-5060.

Fortune, M., 1980: Properties of African squall lines inferred from time-lapse satellite imagery. *Mon. Wea. Rev.*, **108**, 153–168.

Gamache, J.F., and R.A. Houze, 1983: Water budget of a Mesoscale Convective System in the tropics. *J. Atmos. Sci.*, **40**, 1835–1850.

Geerts, B., and T. Dejene, 2005: Regional and diurnal variability of the vertical structure of precipitation systems in Africa based on spaceborne radar data. *J. Climate*, **18**, 893–916.

Gu G., R. F. Adler, G. J. Huffman, and S. Curtis, 2004: African easterly waves and their association with precipitation, *J. Geophys. Res.*, **109**, D04101, doi:10.1029/2003JD003967.

Houze, R.A., 1977: Structure and Dynamics of a Tropical Squall–Line System. *Mon. Wea. Rev.*, **105**, 1540–1567.

Houze, R.A., and C.P. Cheng, 1977: Radar characteristics of tropical convection observed during GATE: Mean properties and trends over the summer season. *Mon. Wea. Rev.*, **105**, 964–980.

Houze, R.A., and E.N. Rappaport, 1984: Air motions and precipitation structure of an early summer squall line over the eastern tropical Atlantic. *J. Atmos. Sci.*, **41**, 553–574.

Hudlow M. D., 1979: Mean rainfall patterns for the three phases of GATE. *J. Appl. Meteor.*, **18**, 1656–1669.

Janicot, S. and co-authors, 2008: Large-scale overview of the summer monsoon over West Africa during the AMMA field experiment in 2006. *Ann. Geophys.*, **26**, 2569-2595.

Keenan, T. D., and R. E. Carbone, 1992: A preliminary morphology of precipitation systems in tropical northern Australia. *Quart. J. Roy. Meteor. Soc.*, **118**, 283-326.

Kiladis, G. N., C. D. Thorncroft, and N. M. J. Hall, 2006: Three-dimensional structure and dynamics of African Easterly Waves. Part I: Observations. *J. Atmos. Sci.*, **63**, 2212-2230.

Laing, A. G., R. Carbone, V. Levizzani, and J. Tuttle, 2008: The propagation and diurnal cycles of deep convection in northern tropical Africa. *Quart. J. Roy. Meteor. Soc.*, **134**, 93-109.

Landsea, C. W., 1993: A climatology of intense (or major) Atlantic hurricanes. *Mon. Wea. Rev.*, **121**, 1703–1713.

Lang, T.J., S.W. Nesbitt, and L.D. Carey, 2009: On the correction of partial beam blockage in polarimetric radar data. *J. Atmos. Oceanic Technol.*, **26**, 943–957.

Leary, C.A., 1984: Precipitation structure of the cloud clusters in a tropical easterly wave. *Mon. Wea. Rev.*, **112**, 313–325.

LeMone, M. A., E. J. Zipser, and S. B. Trier, 1998: The role of environmental shear and thermodynamic conditions in determining the structure and evolution of mesoscale convective systems during TOGA COARE. *J. Atmos. Sci.*, **55**, 3493–3518.

López, R.E., 1978: Internal structure and development processes of C-Scale Aggregates of cumulus clouds. *Mon. Wea. Rev.*, **106**, 1488-1494.

Mathon, V., H. Laurent, and T. Label, 2002: Mesoscale convective system rainfall in the Sahel. *J. Appl. Meteor.*, **41**, 1081-1092.

McTaggart-Cowan, R., G.D. Deane, L.F. Bosart, C.A. Davis, and T.J. Galarneau, 2008:

Climatology of tropical cyclogenesis in the North Atlantic (1948–2004). *Mon. Wea. Rev.*, **136**, 1284–1304.

Mekonnen A., C. D. Thorncroft, and A. R. Aiyyer, 2006: Analysis of convection and its association with African easterly waves. *J. Climate*, **19**, 5405–5421.

Mohr, C.G., L.J. Miller, R.L. Vaughan, and H.W. Frank, 1986: The merger of mesoscale datasets into a common cartesian format for efficient and systematic analyses. *J. Atmos. Oceanic Technol.*, **3**, 143-161.

Nesbitt, S.W., R. Cifelli, and S. A. Rutledge, 2006: Storm morphology and rainfall characteristics of TRMM precipitation features. *Mon. Wea. Rev.*, **134**, 2702-2721.

Nzeukou A., H. Sauvageot, A.D. Ochou, and C. M. F. Kebe, 2004: Raindrop size distribution and radar parameters at Cape Verde. *J. Appl. Meteor.*, **43**, 90–105.

Omotosho J. B., 1985: The separate contributions of squall lines, thunderstorms and the monsoon to the total rainfall in Nigeria. *J. Climatol.*, **5**, 543–552.

Patterson, V. L., M. D. Hudlow, P. J. Pytlowaney, F. P. Richards, and J. D. Hoff, 1979: GATE radar rainfall processing system. NOAA Tech. Memo. EDIS 26, NOAA Washington, D.C., 34 pp. [Available from the National Technical Information Service, Sills Building, 5285 Port Royal Rd., Springfield, VA 22161].

Pytharoulis, I., and C. Thorncroft, 1999: The low-level structure of African Easterly Waves in 1995. *Mon. Wea. Rev.*, **127**, 2266–2280.

Redelsperger, J. L., C. D. Thorncroft, A. Diedhiou, T. Lebel, D. J. Parker, and J. Polcher, 2006: African Monsoon Multidisciplinary Analysis: An International Research Project and Field Campaign. *Bull. Amer. Met. Soc.*, **87**, 1739–1746.

Reed, R. J., D.C. Norquist and E.E. Recker, 1977: The Structure and Properties of African Wave Disturbances as Observed During Phase III of GATE. *Mon. Wea. Rev.*, **105**, 317-333.

Reed, R. J., A. Hollingsworth, W. A. Heckley, and F. Delsol, 1988: An evaluation of the ECMWF operational system in analyzing and forecasting easterly wave disturbances over Africa and the tropical Atlantic. *Mon. Wea. Rev.*, **116**, 824–865

Rickenbach, T.M., and S.A. Rutledge, 1998: Convection in TOGA COARE: Horizontal scale, morphology, and rainfall production. *J. Atmos. Sci.*, **55**, 2715-2729.

Rickenbach, T., R. N. Ferreira, N. Guy, and E. Williams, 2009: Radar-observed squall line propagation and the diurnal cycle of convection in Niamey, Niger during the 2006 AMMA IOP. *J. Geophys. Res.*, **114**, D03107, doi:10.1029/2008JD010871.

Rodger, C. J., J. B. Brundell, and R. L. Dowden, 2005: Location accuracy of VLF World Wide

Lightning Location (WWLL) network: Post-algorithm upgrade. *Ann. Geophys.*, **23**, 277-290.

Ross, R. S., and T. N. Krishnamurti, 2007: Low-level African Easterly Wave activity and its relation to Atlantic tropical cyclogenesis in 2001., *Mon. Wea. Rev.*, **135**, 3950-3964.

Rowell D. P., and J. R. Milford, 1993: On the generation of African squall lines. *J. Climate*, **6**, 1181–1193.

Rutledge S. A., and R. A. Houze Jr., 1987: A diagnostic modeling study of the trailing stratiform region of a midlatitude squall line. *J. Atmos. Sci.*, **44**, 2640–2656.

Sauvageot H., and J.P. Lacaux, 1995: The shape of averaged drop size distributions. *J. Atmos. Sci.*, **52**, 1070–1083.

Schumacher, C. and R. A. Houze, Jr., 2006: Stratiform precipitation production over sub-Saharan Africa and the tropical East Atlantic as observed by TRMM. *Quart. J. Roy. Meteorol. Soc.*, **132**, 2235-2255.

Seo, H., M. Jochum, R. Murtugudde, A.J. Miller, and J.O. Roads, 2008: Precipitation from African Easterly Waves in a Coupled Model of the Tropical Atlantic. *J. Climate*, **21**, 1417–1431.

Steiner, M., R.A. Houze, Jr., and S.E. Yuter, 1995: Climatological characteristics of three-dimensional storm structure from operational radar and raingauge data. *J. Appl. Meteor.*, **34**, 1978-2007.

Thompson R. M. Jr., S. W. Payne, E. E. Recker, and R. J. Reed, 1979: Structure and properties of synoptic-scale wave disturbances in the Intertropical Convergence Zone of the eastern Atlantic. *J. Atmos. Sci.*, **36**, 53–72.

Thorncroft C. D., and K. Hodges, 2001: African easterly wave variability and its relationship to Atlantic tropical cyclone activity. *J. Climate*, **14**, 1166–1179.

Thorncroft, C. D., N. M. J. Hall, and G. N. Kiladis, 2008: Three-dimensional structure and dynamics of African Easterly Waves. Part III: Genesis. *J. Atmos. Sci.*, **65**, 3596-3607.

Yuter, S. E., and R. A. Houze Jr. 1995: Three-dimensional kinematic and microphysical evolution of Florida cumulonimbus. Part II: Frequency distributions of vertical velocity, reflectivity, and differential reflectivity. *Mon. Wea. Rev.*, **123**, 1941–1963.

Wei, T., and R.A. Houze, Jr., 1987: The GATE squall line of 9-10 August 1974. *Advances in Atmos. Sci.*, **4**, 85-92.

Weisman, M. L., and J.B. Klemp, 1986: Characteristics of convective storms. *Mesoscale*

Meteorology and Forecasting, P. S. Ray, Ed., Amer. Meteor. Soc., 331–358.

World Meteorological Organization, 1975: GATE report 17.

Zawislak, J., and E. J. Zipser, 2009: Observations of 7 African Easterly Waves in the east Atlantic during 2006. *J. Atmos. Sci.*, accepted.

Zipser, E., 1977: Mesoscale and convective-scale downdrafts as distinct components of squall-line structure. *Mon. Wea. Rev.*, **105**, 1568–1589.

Zipser, E. J., D. J. Cecil, C. Liu, S. W. Nesbitt, and D. P. Yorty, 2006: Where are the most intense thunderstorms on earth? *Bull. Amer. Meteorol. Soc.*, **87**, 1057–1071.

Zipser, E. J., C. H. Twohy, S.-C. Tsay, K. L. Thornhill, S. Tanelli, R. Ross, T. N. Krishnamurti, Q. Ji, G. Jenkins, S. Ismail, N. C. Hsu, R. Hood, G. M. Heymsfield, A. Heymsfield, J. Halverson, H. M. Goodman, R. Ferrare, J. P. Dunion, M. Douglas, R. Cifelli, G. Chen, E. V. Browell, and B. Anderson: The Saharan air layer and the fate of African Easterly Waves. NASA's AMMA 2006 field program to study tropical cyclogenesis: NAMMA, *Bull. Amer. Meteor. Soc.*, in press.

Figure Captions

1. Approximate location of Wave 5 from 31 August – 4 September 2006. Horizontal (vertical) axis is longitude (latitude) in degrees. Filled circles (triangles) indicate vorticity maxima at 700 (925) mb and dashed lines show the approximate position of the 700 mb trough line at 00 UTC, based on ECMWF operational analyses. Shading represents the day of the month. Rectangles labeled T, N, and M indicate the domain of the TOGA, NPOL, and MIT radar sites.
2. (a) Time-longitude diagram of 700 mb meridional wind for the time period 25 August – 5 September 2006, based on ECMWF operational analysis. The meridional winds have been averaged over the latitude domain of 10-20°N at 6-hour intervals. Dark (light) shading indicates southerly (northerly) winds. The “W5” in the lower right hand corner indicates the approximate position of the Wave 5 trough. The location of the 3 radar sites are indicated by the vertical dashed lines and represent, from left to right, TOGA (oceanic), NPOL (coastal), and MIT (continental). (b) same as (a) except for fraction of rain rates above 1 mm hr⁻¹, averaged over 12-17°N at 3-hour intervals. Rain rates are from the TRMM 3B42 product. The symbols “1”, “2”, and “3” indicate the propagating events described in the text. The approximate tracks of the events are indicated by the solid lines sloping from the lower right to upper left part of the figure. Horizontal dashed lines refer to the approximate local time interval for day (indicated by “D” - 06:00-18:00 L) and night (indicated by “N” - 18:00-06:00 L), respectively. Arrows represent the average position of the Joss Plateau (8°E) and Guinea Highlands (12°W).

3. Time series of (a) meridional wind (b) zonal wind, (c) relative humidity, and (d) CAPE at Niamey, Niger from 30 August 00 UTC – 2 September 06 UTC, based on upper air sounding data. White areas represent missing data. The dotted lines in each panel indicate the approximate time intervals that each precipitation event (indicated by “E1”, “E2”, and “E3”) was sampled by the MIT radar. The arrows indicate the approximate time of the trough passage. Shading in panel (d) indicates the approximate daytime period.

4. Low-level Plan Position Indicator (PPI) scans of radar reflectivity from the MIT radar at (a) 0701 UTC 30 August, 2006 (Event 1), (b) 0101 UTC 31 August 2006, (Event 2) (c) 1311 UTC 31 August, 2006 (Event 2), and (d) 0601 UTC 1 September 2006 (Event 3).

5. ECMWF analysis at (a) 00 UTC 30 August, 2006, (b) 12 UTC 30 August, 2006, and (c) 00 UTC 31 August, 2006, and (d) 12 UTC 31 August, 2006. Northerly (southerly) wind at 700 mb is indicated by the dark (light) shading. Convergence at 925 mb is contoured in solid lines starting at $0.1 \times 10^{-4} \text{ s}^{-1}$. Relative vorticity is contoured in dashed lines starting at $0.25 \times 10^{-5} \text{ s}^{-1}$. Lightning flash locations within one hour of the ECMWF analysis times are shown by the ‘+’ symbols. The dotted line is the approximate position of the AEJ based on the 700 mb zonal wind. The MIT radar (Niamey) domain is indicated by the rectangle. Panels (a) and (b) refer to Event 1. Panels (c) and (d) refer to Event 2.

6. Same as Fig. 3, except for Dakar, Senegal between 06 UTC 1 September, 2006 and 15

UTC 3 September, 2006.

7. Figure 7. Same as Fig. 4, except for NPOL radar (a) and (b) 0100 UTC on 2 September, 2006 (Event 2) and (c) 1601 UTC on 2 September 2006 (Event 3). Panel (b) shows radial velocity in m s^{-1} . Flow toward (away) from the radar is indicated by negative (positive) values.
8. . Same as Fig. 5, except for September 2, 2006. The rectangle represents the NPOL radar (Dakar) sampling domain. Panels (a) and (b) refer to Event 2. Panels (c) and (d) refer to Event 3.
9. Same as Fig. 3, except for Praia, Cape Verde between 03 UTC 2 September, 2006 and 0730 UTC 5 September, 2006.
10. Same as Fig. 4, except for the TOGA radar (a) 2 September, 2006 2341 UTC and (b) 3 September, 2006 1401 UTC.
11. Same as Fig. 5, except for 3 September, 2006. The rectangle represents the TOGA radar (Praia) sampling domain.
12. Time series of (left) total convective and (right) total stratiform radar echo area sampled at Niamey (top row), Dakar, (middle row), and Praia (bottom row). relative to the 700 mb trough passage at each site. The vertical dotted lines bracket the time period that each

propagating event (labeled as “E1”, “E2”, and “E3”) was sampled by the radar. The solid vertical line indicates the time of the 700 mb trough passage.

13. Same as Fig. 12 except for rain volume.

14. . Similar to Fig. 12, except for flash count from the WWLLN network. The flashes are divided into 1-hour time bins (smoothed with a 3-point moving average filter) and are representative of a 5 x 5 deg area centered on the location of each radar site.

15. Rain volume contribution (%) as a function of mean maximum 20 dBZ echo top height for (a) MCS features, and (b) sub-MCS features.

16. Contoured frequency by altitude diagrams (CFADs) of radar reflectivity for (top) convective and (bottom) stratiform precipitation during the passage of Wave 5. The columns represent (left) Praia-oceanic, (middle) Dakar-coastal, and (right) Niamey-continental radar data. Increasing relative frequency of occurrence of radar reflectivity at each altitude is indicated by shading as indicated in the gray-scale bar. Mean profiles of radar reflectivity are indicated by the solid black line in each panel.

Table 1. Time of influence of Wave 5 at each radar location.

Location	Time period of Wave 5 influence	Time of 700 mb Trough Passage
Niamey (MIT radar)	30 Aug. 06Z – 2 Sep. 06Z	31 Aug. 03Z
Dakar (NPOL radar)	1 Sep. 18Z – 4 Sep. 06Z	2 Sep. 06Z
Praia (TOGA radar)	2 Sep. 06Z – 5 Sep. 06Z	3 Sep. 12Z

Table 2. Sampling Characteristics of the MIT, NPOL, and TOGA radars.

	TOGA	NPOL	MIT
3 dB beam width	1.66°	1.00°	1.40°
Pulse Repetition Frequency	1001 Hz	950 Hz	950 Hz
Repeat Cycle	10 min	15 min	10 min
Wavelength	0.053 m	.107 m	0.053 m
Range gate size	150 m	200 m	250 m
Unambiguous Range	150 km	157 km	158 km
Pulse Width	0.8 us	0.8 us	1.0 us

Table 3. Area and rain volume fractions for MCS features compared to all features and convective rain compared to total (convective + stratiform) rain.

Location	MCS area fraction (%)	MCS rain volume fraction (%)	*Convective area fraction (%)	*Convective rain volume fraction(%)
Continental (MIT)	78	87	14	52
Coastal (NPOL)	69	84	13	72
Oceanic (TOGA)	72	89	17	71
Average	73	87	15	65

* all features (MCS + sub-MCS + NC)

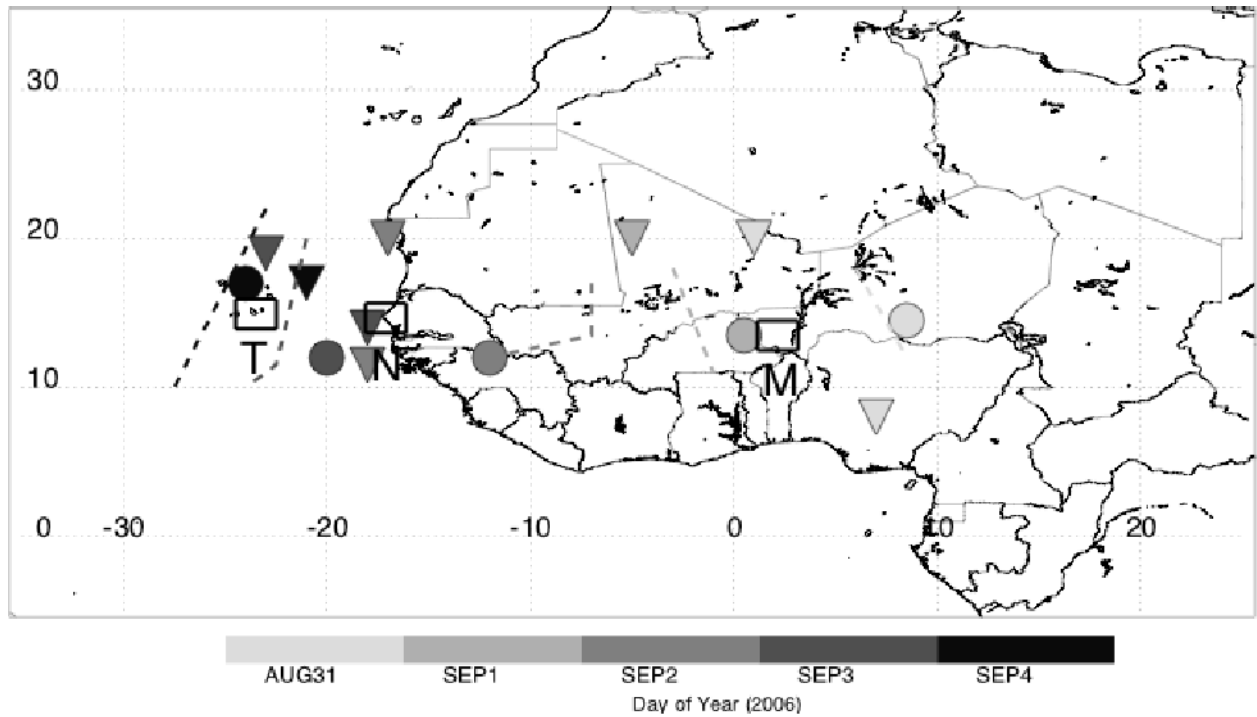
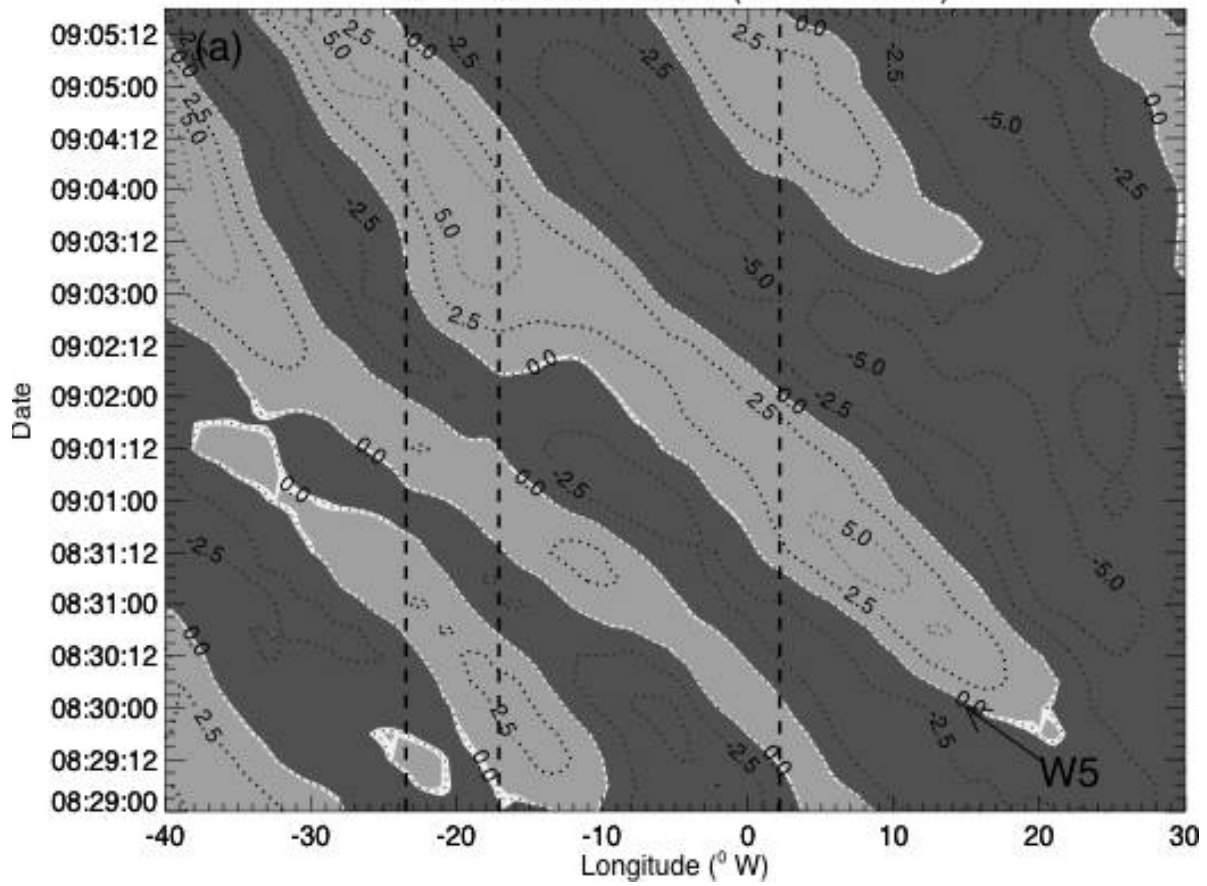


Figure 1. Approximate location of Wave 5 from 31 August – 4 September 2006. Horizontal (vertical) axis is longitude (latitude) in degrees. Filled circles (triangles) indicate vorticity maxima at 700 (925) mb and dashed lines show the approximate position of the 700 mb trough line at 00 UTC, based on ECMWF operational analyses. Shading represents the day of the month. Rectangles labeled T, N, and M indicate the domain of the TOGA, NPOL, and MIT radar sites.

Mean 700 mb VWND (10° N - 20° N)



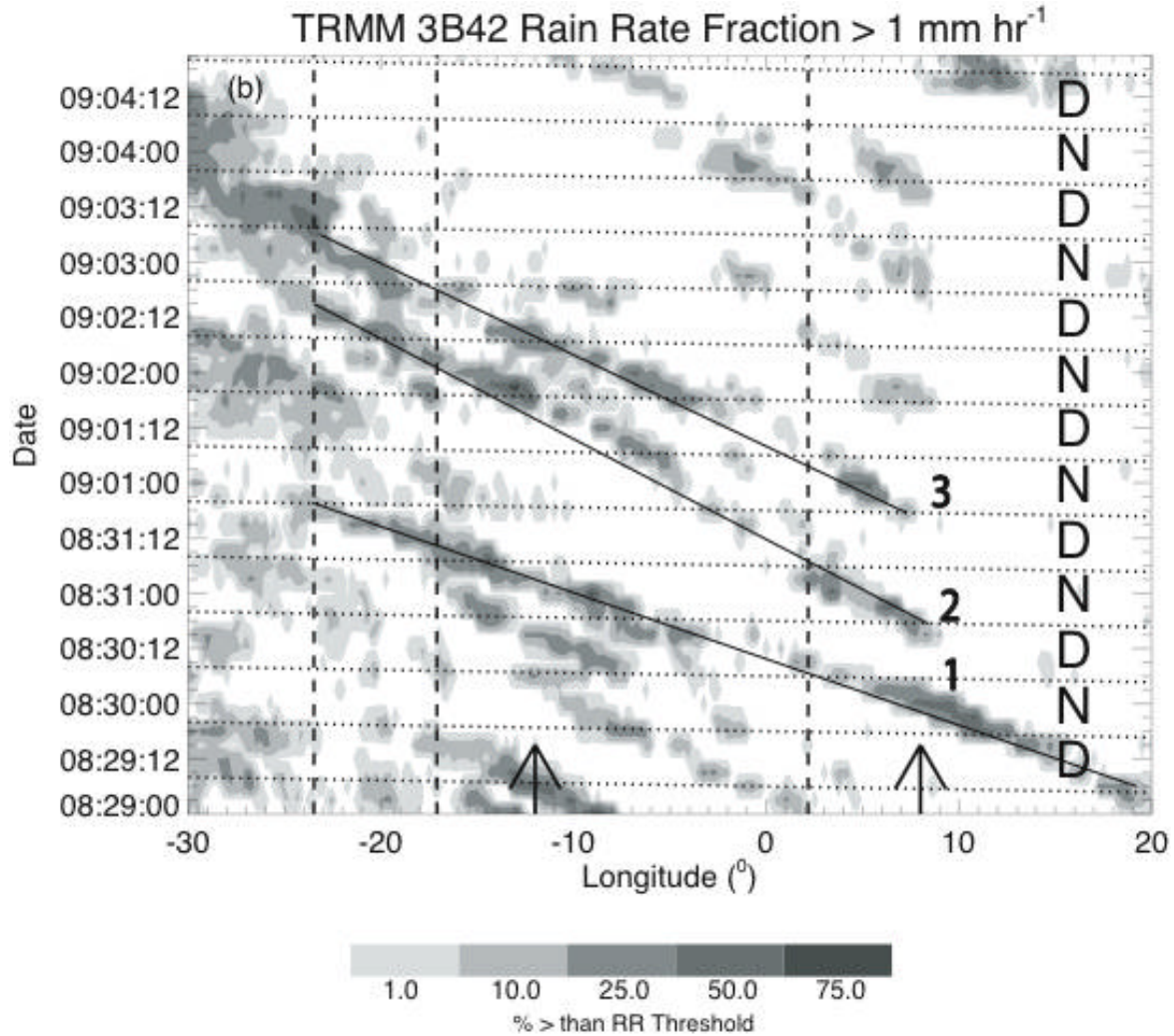


Figure 2. (a) Time-longitude diagram of 700 mb meridional wind for the time period 25 August – 5 September 2006, based on ECMWF operational analysis. The meridional winds have been averaged over the latitude domain of 10-20°N at 6-hour intervals. Dark (light) shading indicates southerly (northerly) winds. The “W5” in the lower right hand corner indicates the approximate position of the Wave 5 trough. The location of the 3 radar sites are indicated by the vertical dashed lines and represent, from left to right, TOGA (oceanic), NPOL (coastal), and MIT (continental). (b) same as (a) except for fraction of rain rates above 1 mm hr⁻¹, averaged over 12-17°N at 3-hour intervals. Rain rates are from the TRMM 3B42 product. The symbols “1”, “2”,

and “3” indicate the propagating events described in the text. The approximate tracks of the events are indicated by the solid lines sloping from the lower right to upper left part of the figure. Horizontal dashed lines refer to the approximate local time interval for day (indicated by “D” - 06:00-18:00 L) and night (indicated by “N” - 18:00-06:00 L), respectively. Arrows represent the average position of the Joss Plateau (8°E) and Guinea Highlands (12°W).

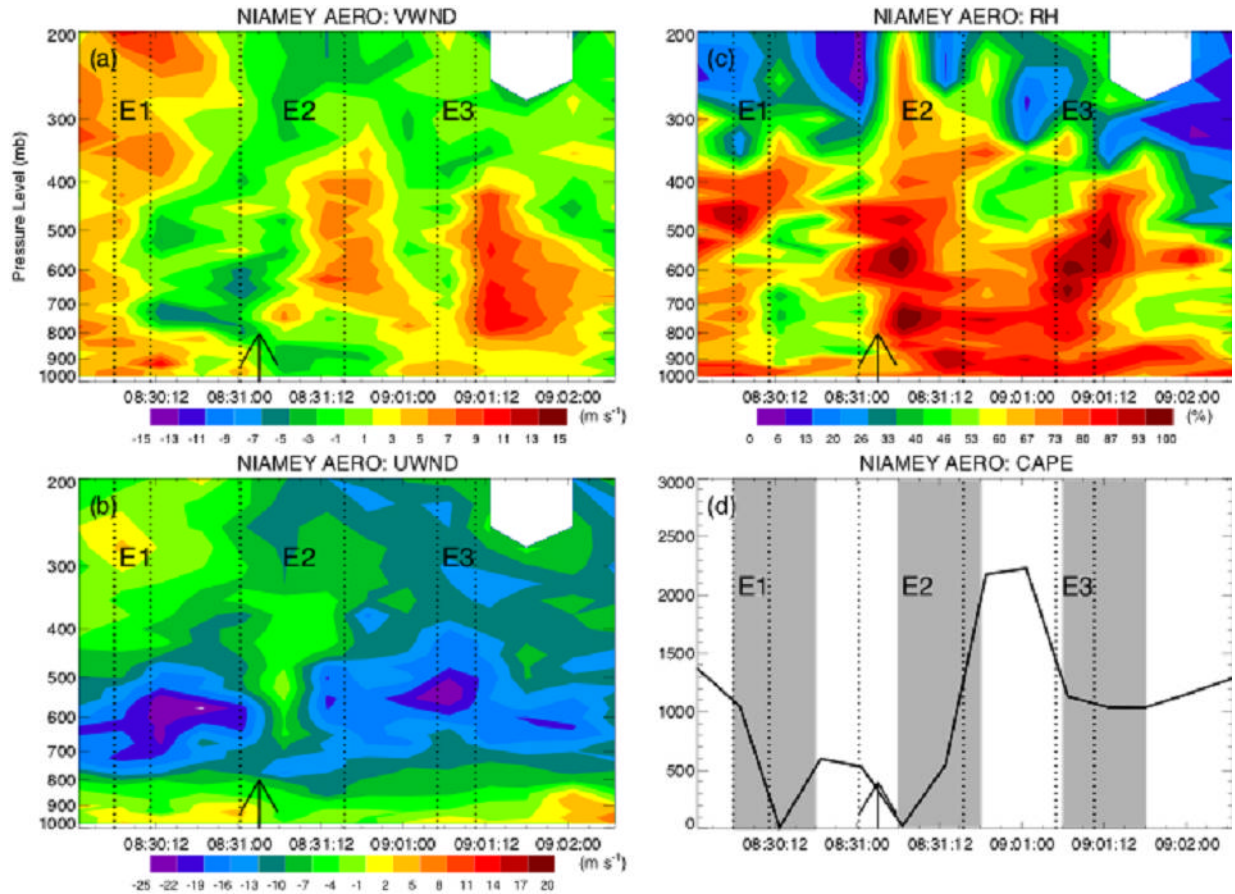


Figure 3. Time series of (a) meridional wind (b) zonal wind, (c) relative humidity, and (d) CAPE at Niamey, Niger from 30 August 00 UTC – 2 September 06 UTC, based on upper air sounding data. White areas represent missing data. The dotted lines in each panel indicate the approximate time intervals that each precipitation event (indicated by “E1”, “E2”, and “E3”) was sampled by the MIT radar. The arrows indicate the approximate time of the trough passage. Shading in panel (d) indicates the approximate daytime period.

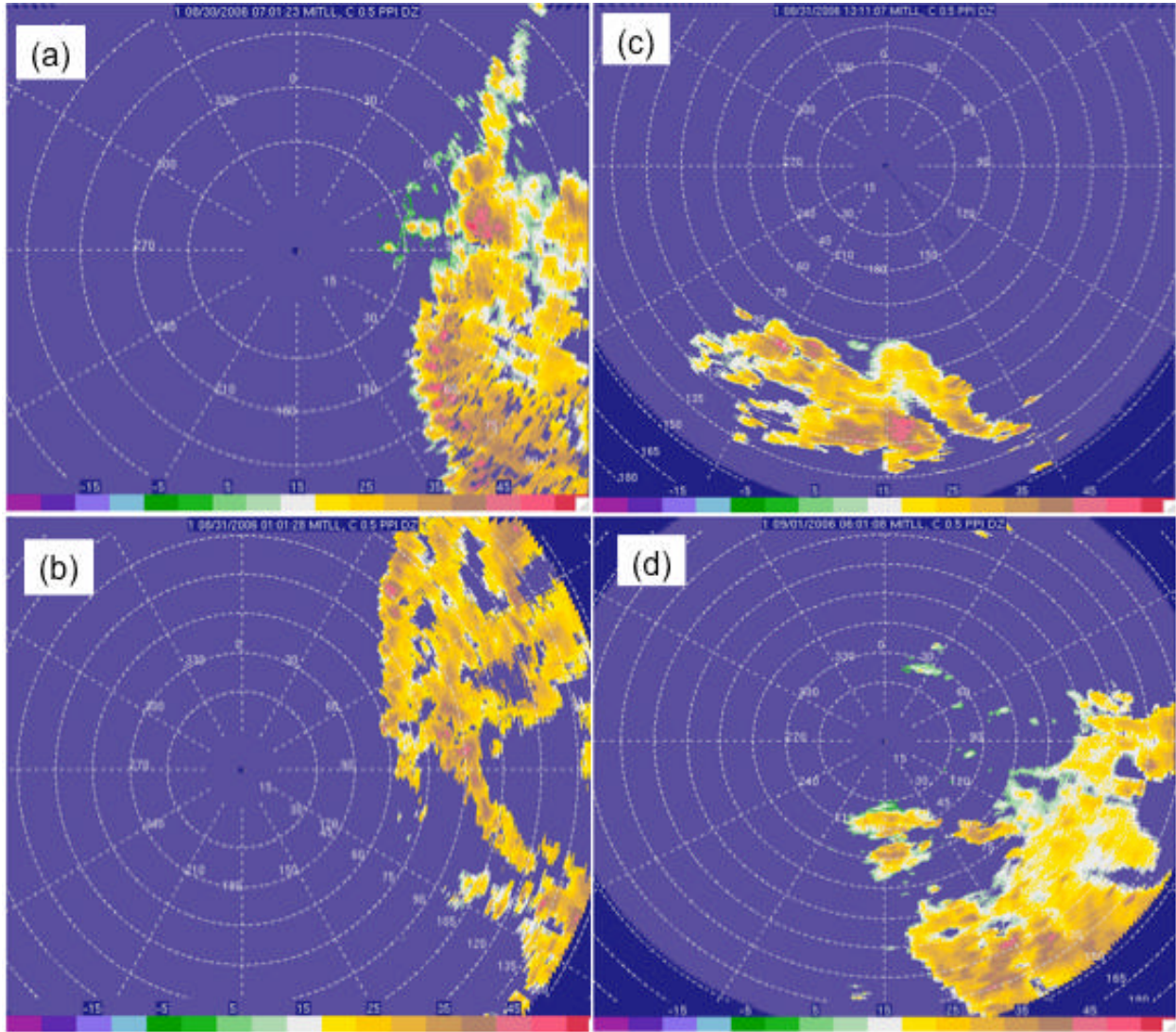


Figure 4. Low-level Plan Position Indicator (PPI) scans of radar reflectivity from the MIT radar at (a) 0701 UTC 30 August, 2006 (Event 1), (b) 0101 UTC 31 August 2006 (Event 2), (c) 1311 UTC 31 August, 2006 (Event 2), and (d) 0601 UTC 1 September 2006 (Event 3).

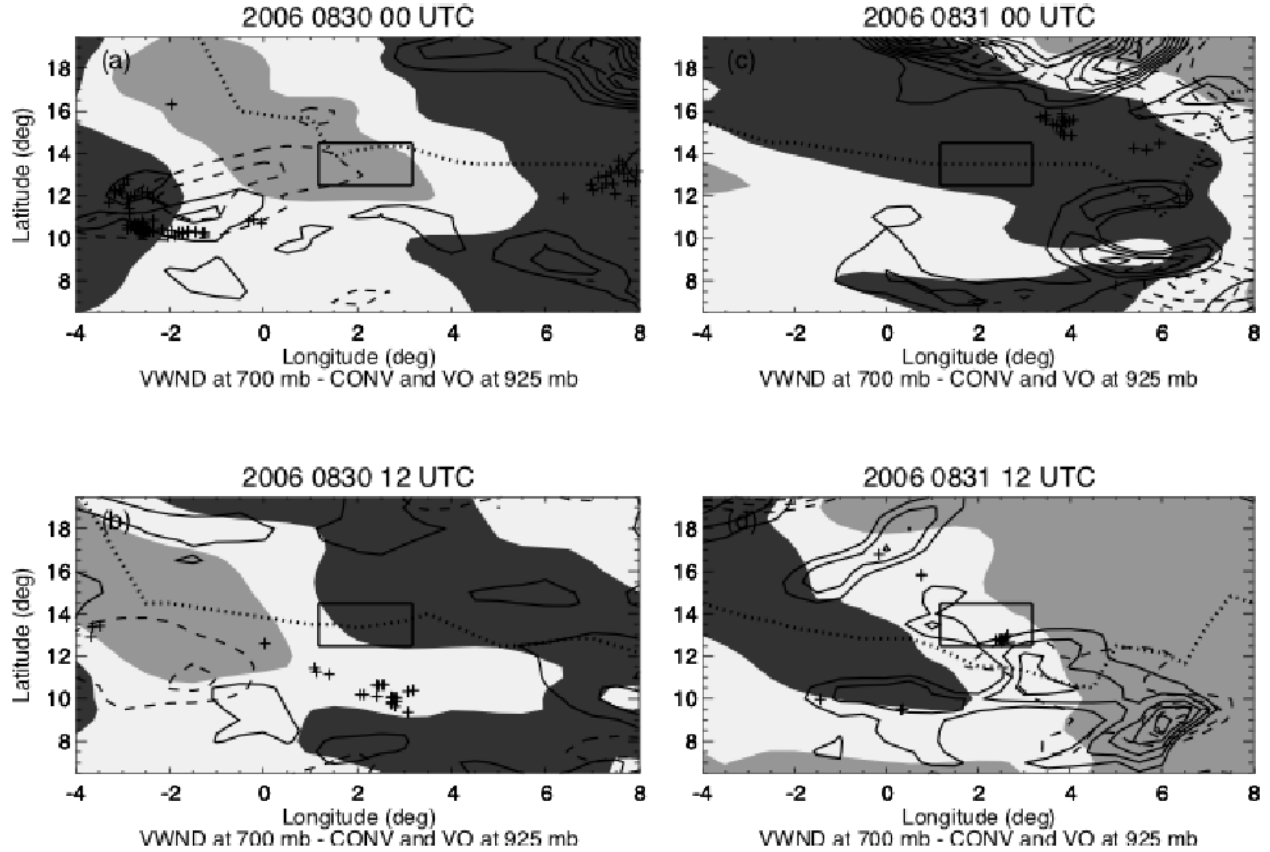


Figure 5. ECMWF analysis at (a) 00 UTC 30 August, 2006, (b) 12 UTC 30 August, 2006, and (c) 00 UTC 31 August, 2006, and (d) 12 UTC 31 August, 2006. Northerly (southerly) wind at 700 mb is indicated by the dark (light) shading. Convergence at 925 mb is contoured in solid lines starting at $0.1 \times 10^{-4} \text{ s}^{-1}$. Relative vorticity is contoured in dashed lines starting at $0.25 \times 10^{-5} \text{ s}^{-1}$. Lightning flash locations within one hour of the ECMWF analysis times are shown by the '+' symbols. The dotted line is the approximate position of the AEJ based on the 700 mb zonal wind. The MIT radar (Niamey) domain is indicated by the rectangle. Panels (a) and (b) refer to Event 1. Panels (c) and (d) refer to Event 2.

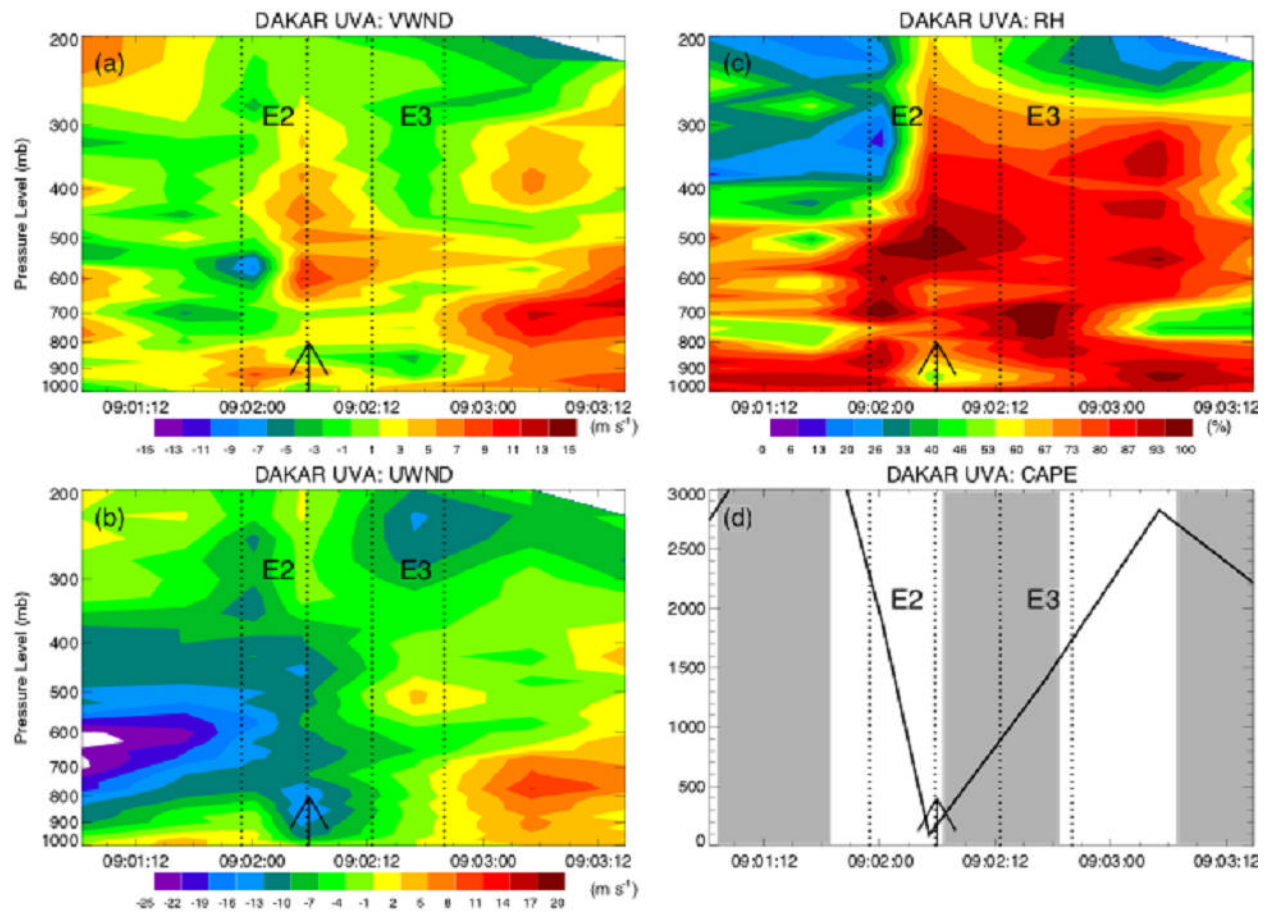


Figure 6. Same as Fig. 3, except for Dakar, Senegal between 06 UTC 1 September, 2006 and 15 UTC 3 September, 2006.

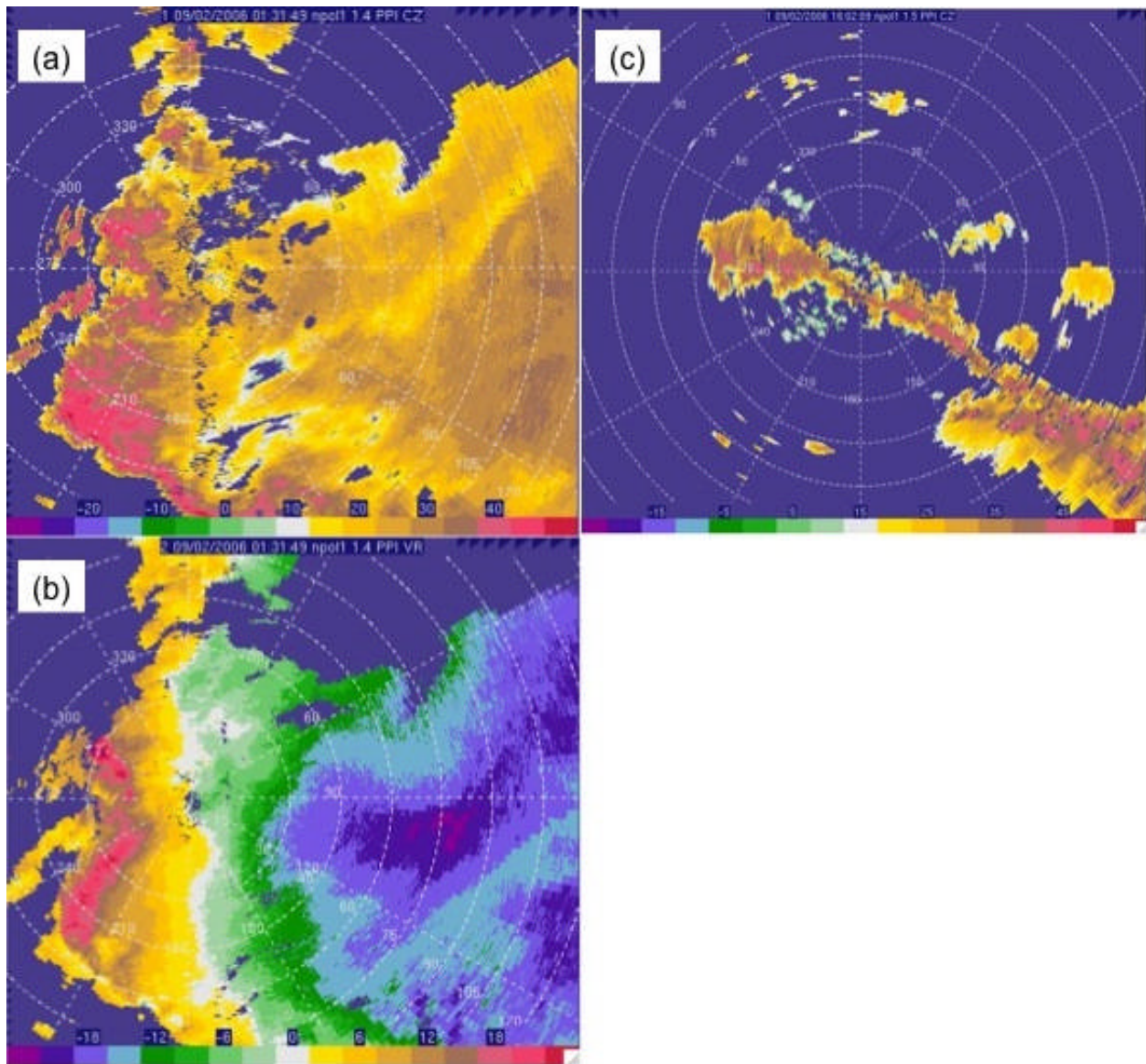


Figure 7. Same as Fig. 4, except for NPOL radar (a) and (b) 0100 UTC on 2 September, 2006 (Event 2) and (c) 1601 UTC on 2 September 2006 (Event 3). Panel (b) shows radial velocity in m s^{-1} . Flow toward (away) from the radar is indicated by negative (positive) values.

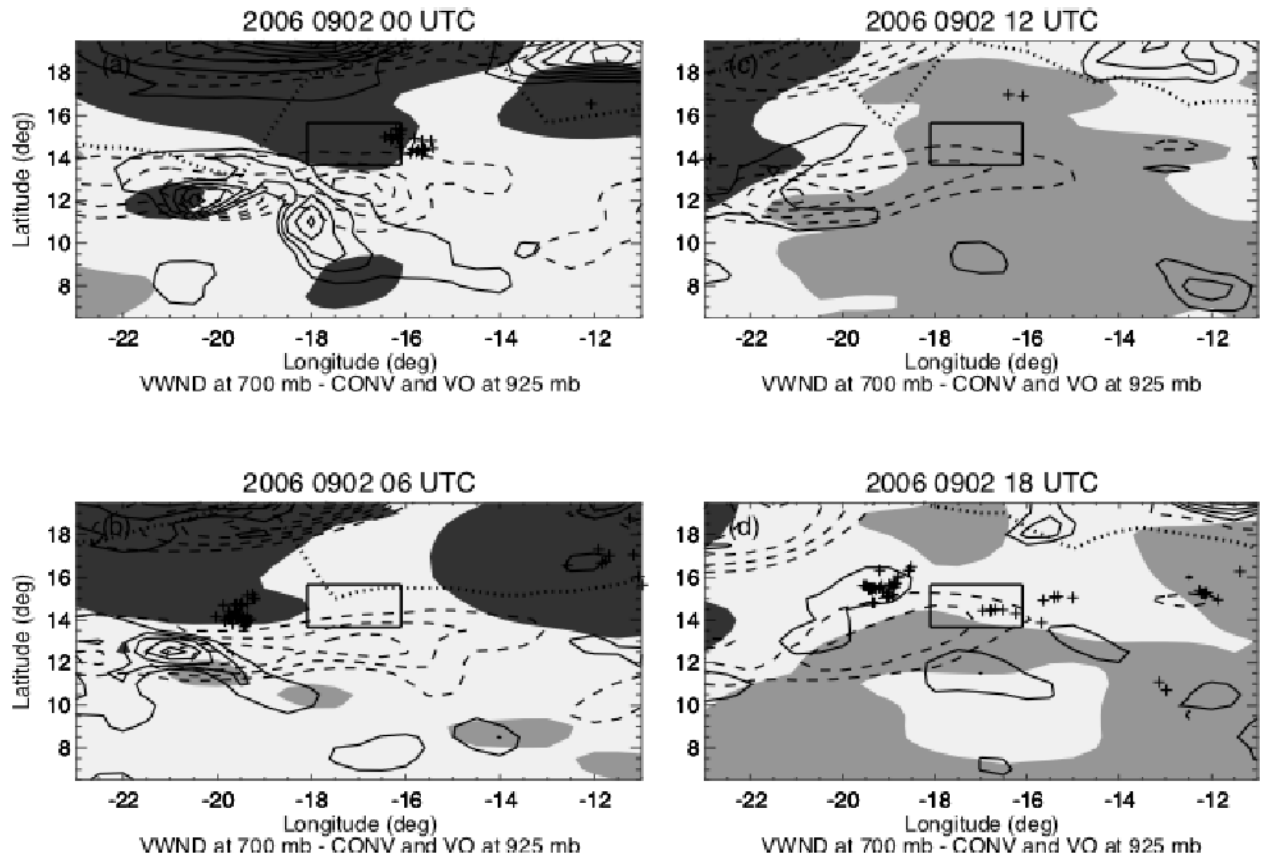


Figure 8. Same as Fig. 5, except for September 2, 2006. The rectangle represents the NPOL radar (Dakar) sampling domain. Panels (a) and (b) refer to Event 2. Panels (c) and (d) refer to Event 3.

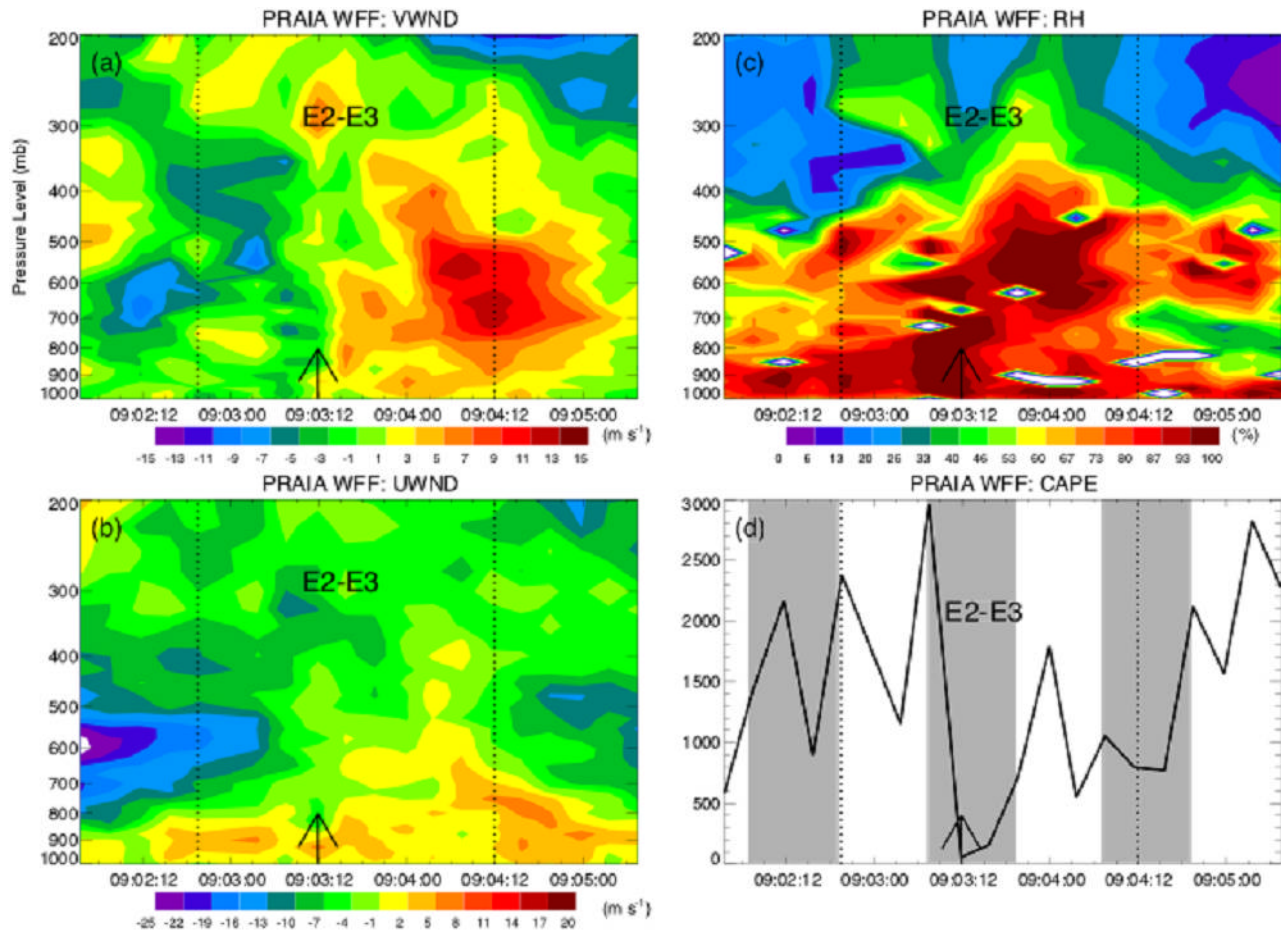


Figure 9. Same as Fig. 3, except for Praia, Cape Verde between 03 UTC 2 September, 2006 and 0730 UTC 5 September, 2006.

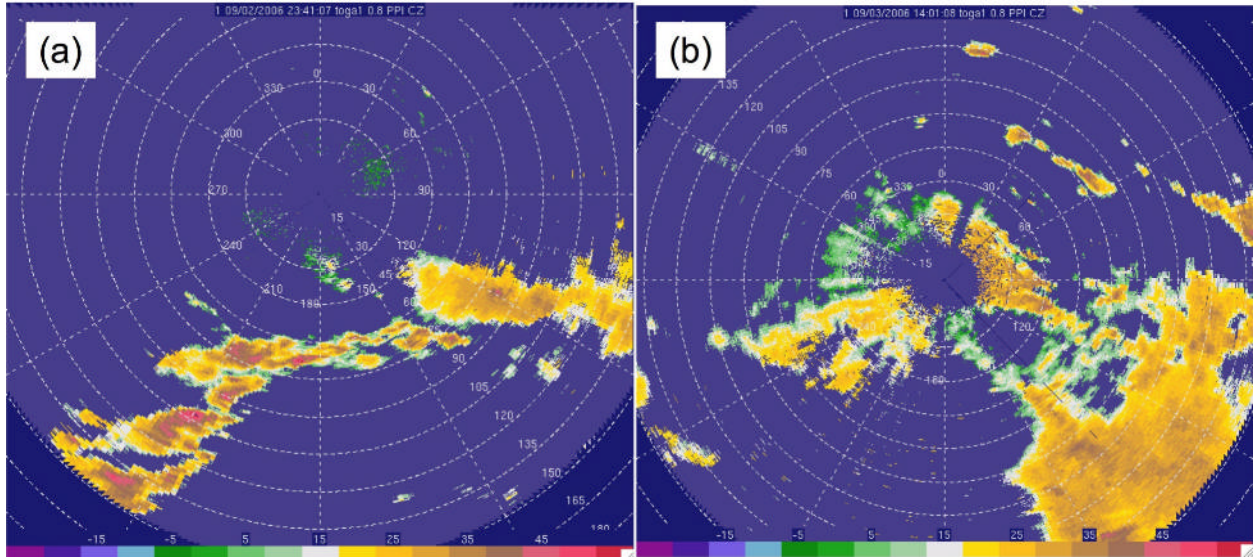


Figure 10. Same as Fig. 4, except for the TOGA radar (a) 2 September, 2006 2341 UTC and (b) 3 September, 2006 1401 UTC.

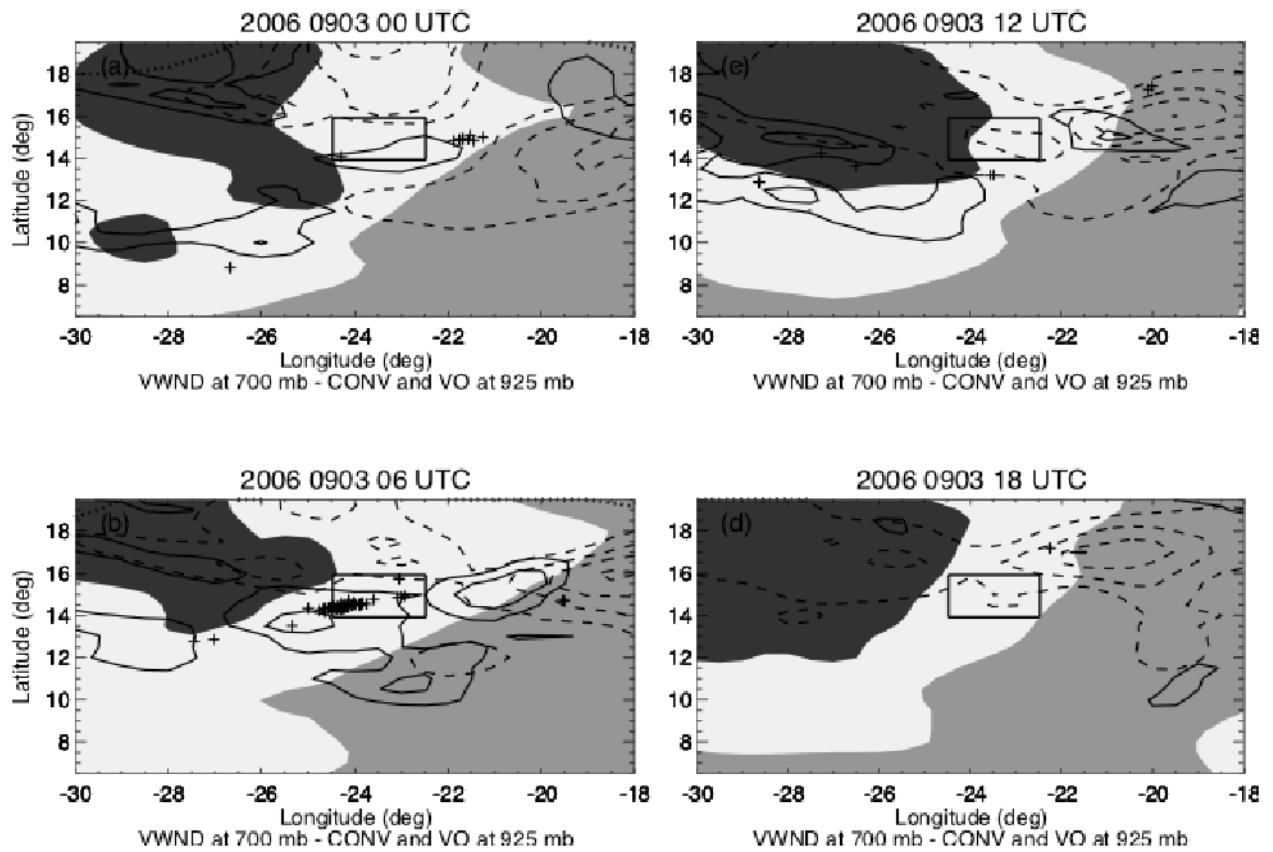


Figure 11. Same as Fig. 5, except for 3 September, 2006. The rectangle represents the TOGA radar (Praia) sampling domain.

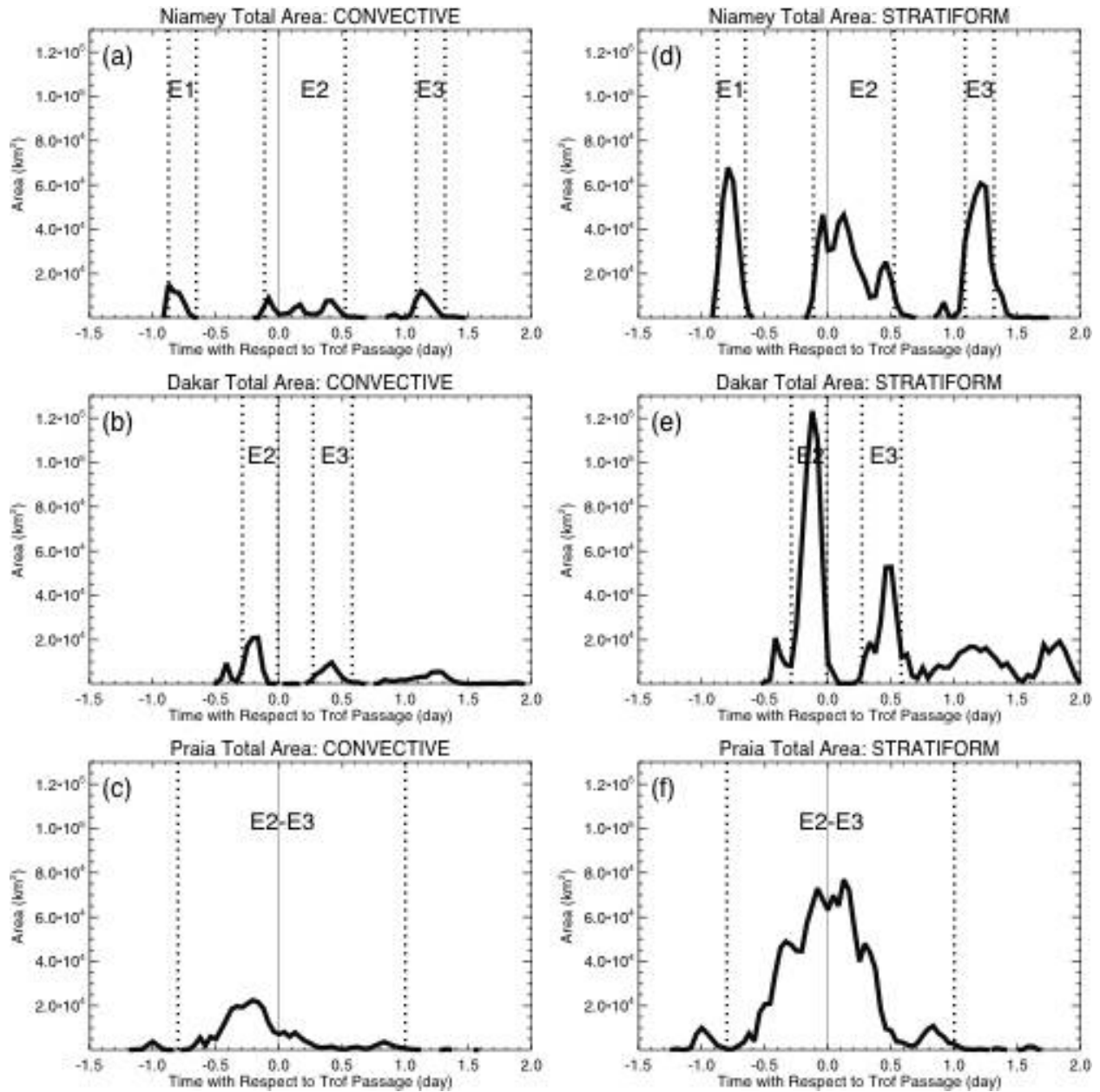


Figure 12. Time series of (left) total convective and (right) total stratiform radar echo area sampled at Niamey (top row), Dakar, (middle row), and Praia (bottom row). relative to the 700 mb trough passage at each site. The vertical dotted lines bracket the time period that each propagating event (labeled as “E1”, “E2”, and “E3”) was sampled by the radar. The solid vertical line indicates the time of the 700 mb trough passage.

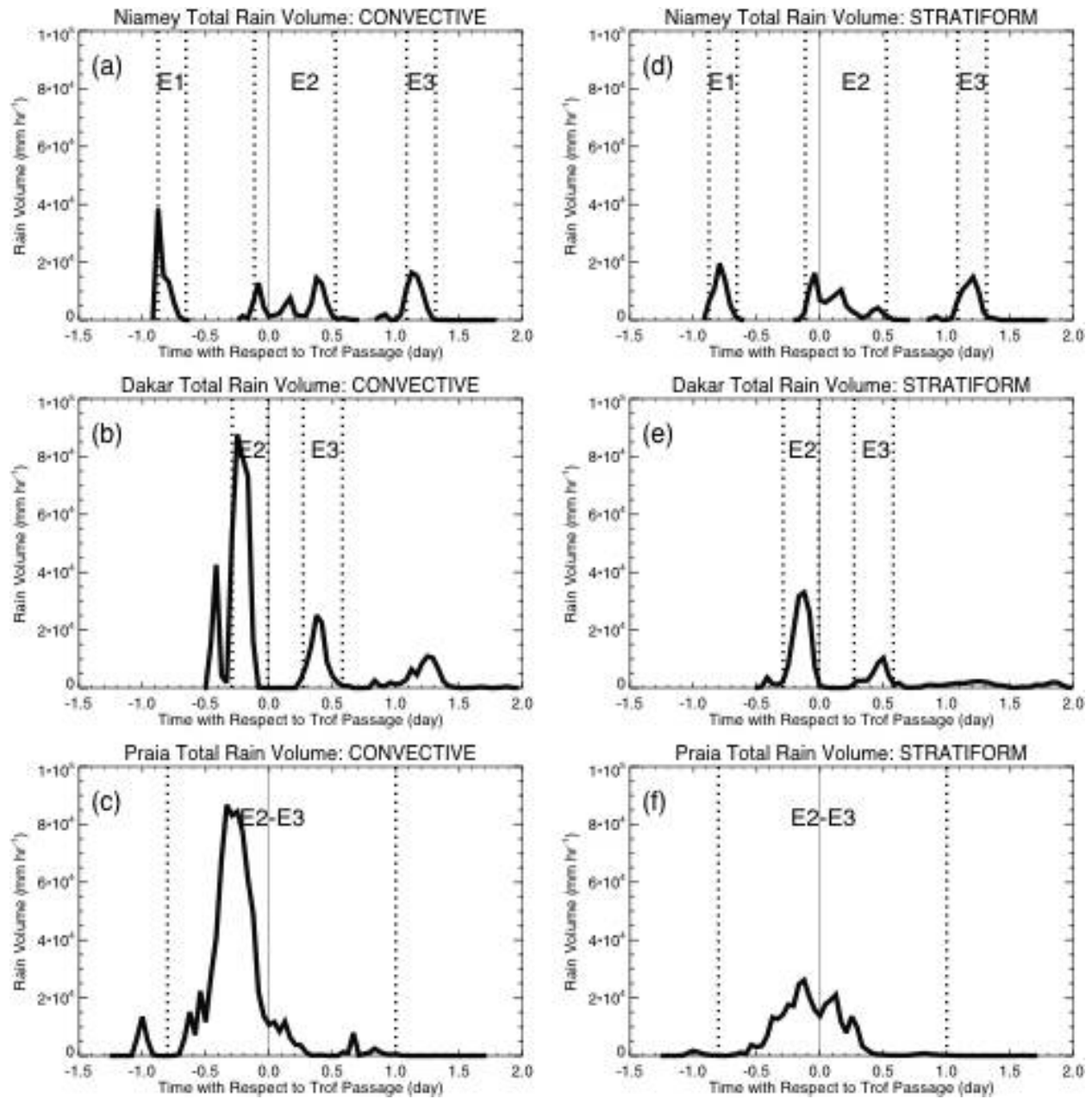


Figure 13. Same as Fig. 12 except for rain volume.

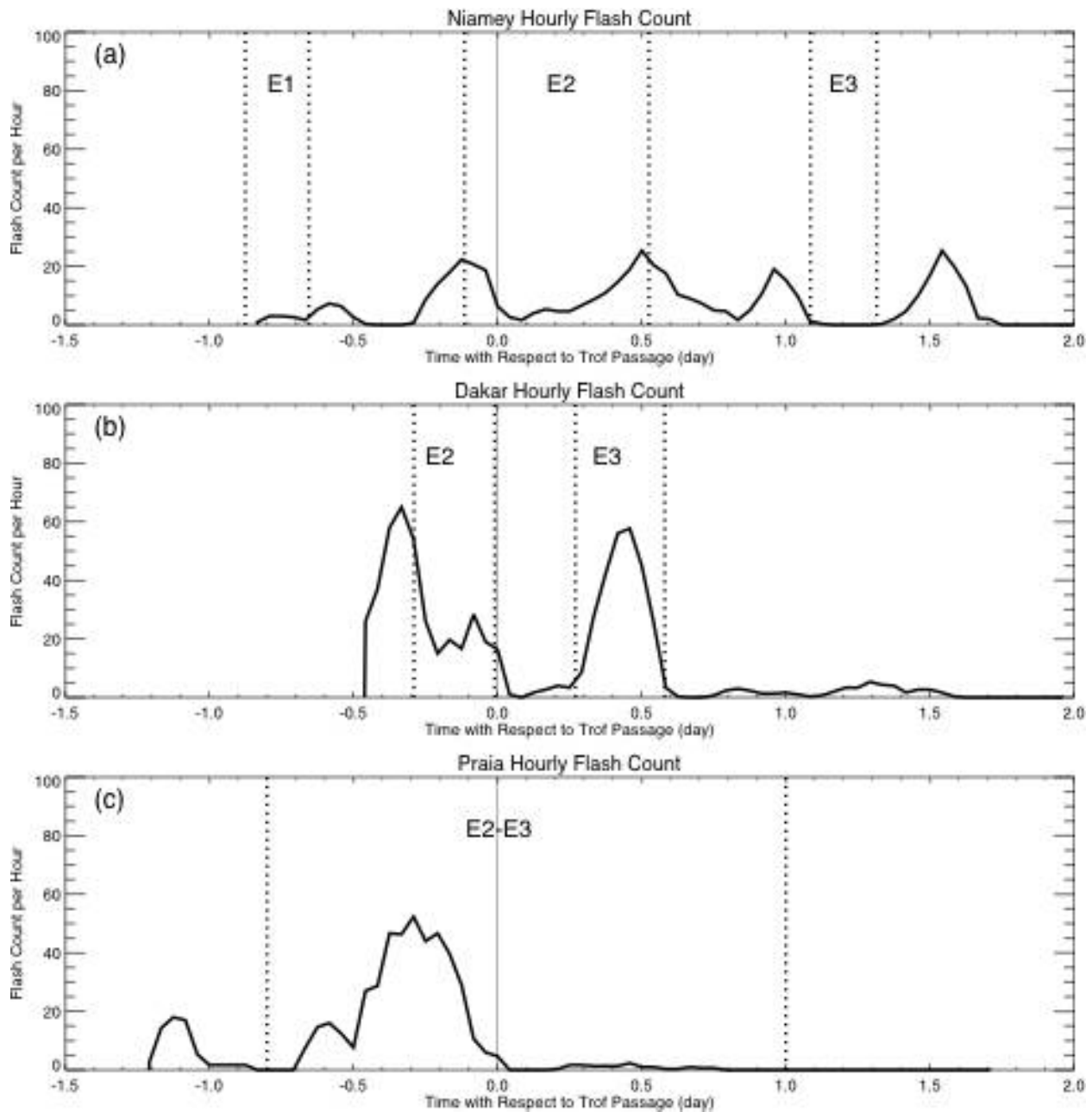


Figure 14. Similar to Fig. 12, except for flash count from the WWLLN network. The flashes are divided into 1-hour time bins (smoothed with a 3-point moving average filter) and are representative of a 5 x 5 deg area centered on the location of each radar site.

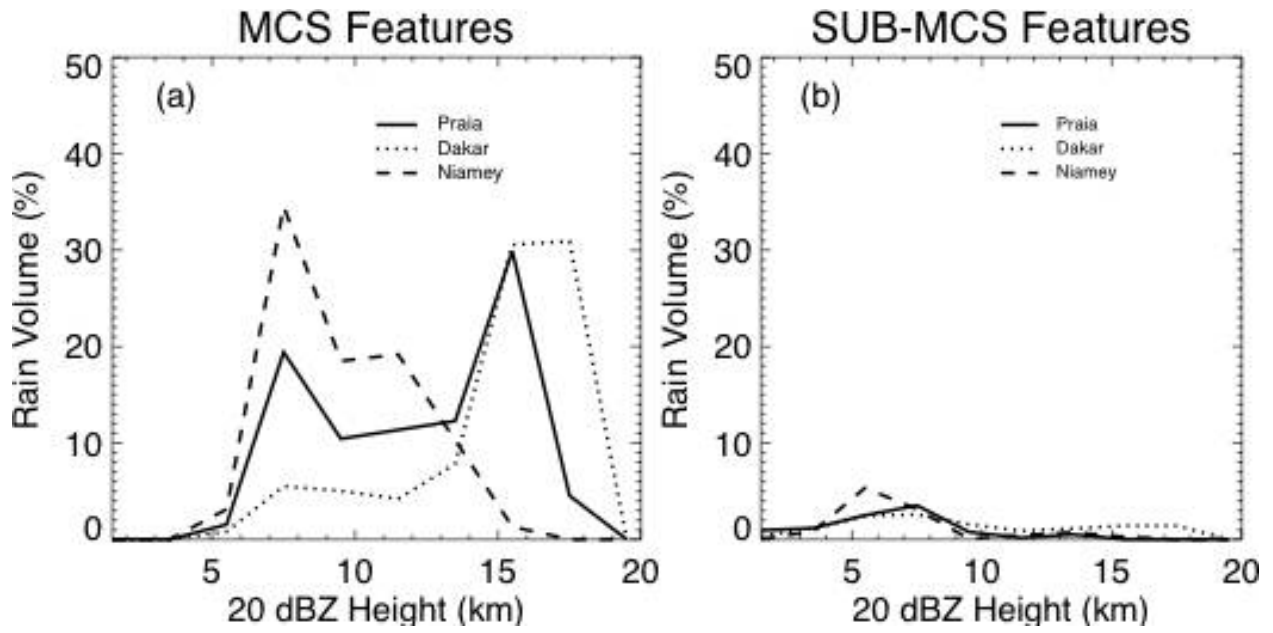


Figure 15. Rain volume contribution (%) as a function of mean maximum 20 dBZ echo top height for (a) MCS features, and (b) sub-MCS features.

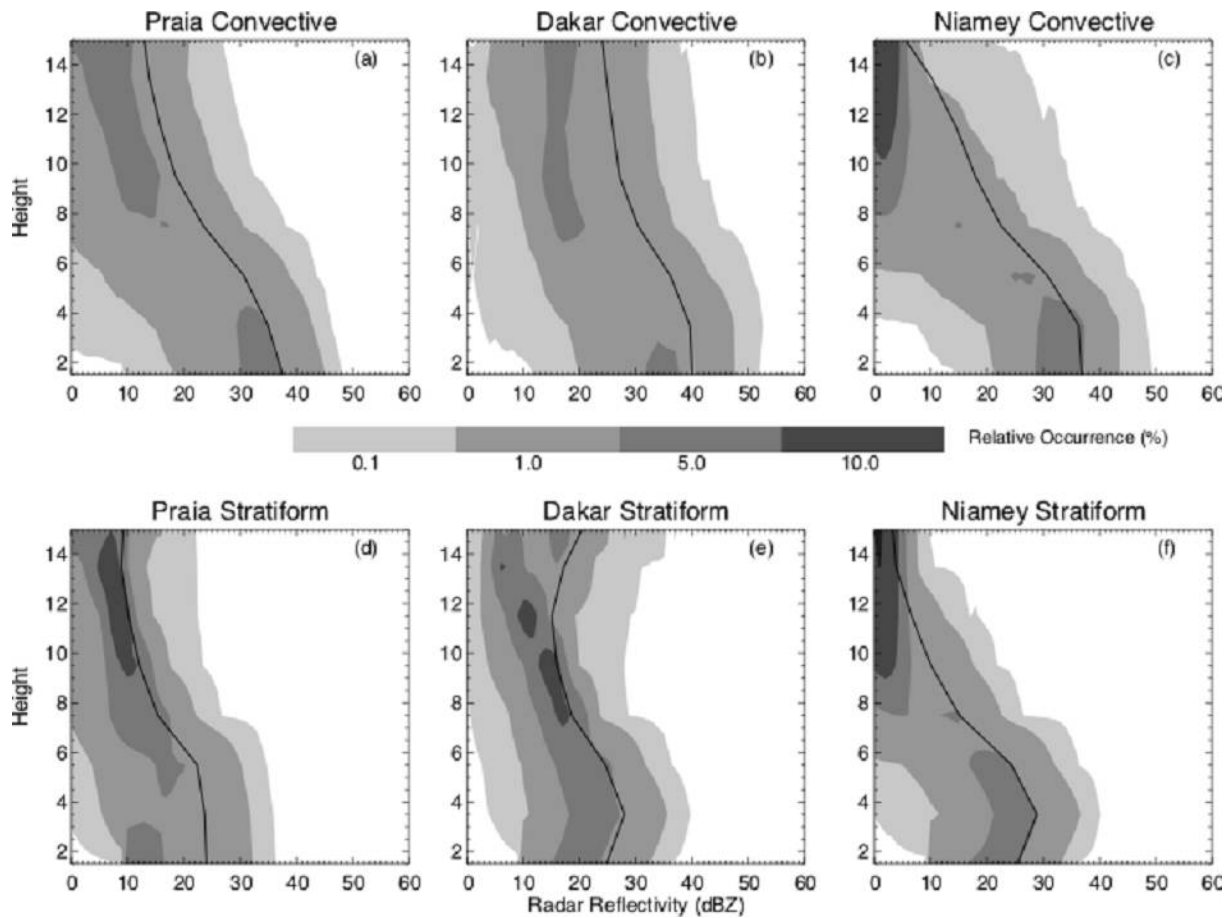


Figure 16. Contoured frequency by altitude diagrams (CFADs) of radar reflectivity for (top) convective and (bottom) stratiform precipitation during the passage of Wave 5. The columns represent (left) Praia-oceanic, (middle) Dakar-coastal, and (right) Niamey-continental radar data. Increasing relative frequency of occurrence of radar reflectivity at each altitude is indicated by shading as indicated in the gray-scale bar. Mean profiles of radar reflectivity are indicated by the solid black line in each panel.